NIST Technical Note
NIST TN 2233

Validation of and Optimization with a Vapor Compression Cycle Model Accounting for Refrigerant Thermodynamic and Transport Properties

With Focus on Low Global-Warming-Potential Refrigerants

Harrison Skye
Piotr Domanski
Riccardo Brignoli
Sanghun Lee
Heunghee Bae

This publication is available free of charge from:
https://doi.org/10.6028/NIST.TN.2233

NATIONAL INSTITUTE OF STANDARDS AND TECHNOLOGY
U.S. DEPARTMENT OF COMMERCE

NIST Technical Note
NIST TN 2233

Validation of and Optimization with a Vapor Compression Cycle Model Accounting for Refrigerant Thermodynamic and Transport Properties

With Focus on Low Global-Warming-Potential Refrigerants

Harrison Skye
Building and Environment Division
Engineering Laboratory, NIST

Piotr Domanski
Building and Environment Division
Engineering Laboratory, NIST

Riccardo Brignoli
VIS Engineering, Padova (PD), Italy

Sanghun Lee
LG Electronics, Air-Solutions Business Unit, South Korea

Heunghee Bae
LG Electronics, Air-Solutions Business Unit, South Korea

This publication is available free of charge from:
https://doi.org/10.6028/NIST.TN.2233

September 2022

U.S. Department of Commerce
Gina M. Raimondo, Secretary

National Institute of Standards and Technology
Laurie E. Locascio, NIST Director and Under Secretary of Commerce for Standards and Technology

NIST Technical Note 2233
September 2022

NIST Technical Series Policies

Publication History
Approved by the NIST Editorial Review Board on 2022-08-29

How to Cite this NIST Technical Series Publication
Skye H, Domanski P, Brignoli R, Lee S, Bae H (2022) Validation of and Optimization with a Vapor Compression Cycle Model Accounting for Refrigerant Thermodynamic and Transport Properties. (National Institute of Standards and Technology, Gaithersburg, MD), NIST Technical Note (TN) 2233. https://doi.org/10.6028/NIST.TN.2233

NIST Author ORCID iDs
Harrison Skye: 0000-0001-6118-0699
Piotr Domanski: 0000-0003-1915-2170
Riccardo Brignoli: 0000-0002-6005-7258
Sanghun Lee: 0000-0001-7820-2444

Contact Information
harrison.skye@nist.gov

Abstract

CYCLE_D-HX is a semi-theoretical model that simulates the performance of a vapor-compression cycle with forced-convection heat exchangers for specified temperature profiles of the heat source and heat sink. In this study, we validated CYCLE_D-HX using experimental measurements from a small (< 4 kW capacity) heat pump test apparatus operated in cooling mode. We also applied the model to simulate the performance of selected refrigerants in a system with optimized refrigerant circuitries in the evaporator and condenser. The tested refrigerants included the medium-pressure refrigerant R-134a and candidate replacements with a lower global-warming potential (GWP): R-513A, R-450A, R-134a/1234yf/1234ze(E) (49.2/33.8/17.0 mass fraction, %), R-515B, and R-1234yf. We also tested high-pressure refrigerant R-410A and candidate replacements with lower-GWP: R-32, R-452B, and R-454B. The model generally agreed with experimental results, with COP and Q_{vol} overpredicted by (0 to 3) % for the basic cycle, and by (0 to 5) % for the cycle with the liquid-line/suction-line heat exchanger (LLSL-HX). Simulations with equal compressor efficiency and optimized tube circuitry showed the COP spread among medium-pressure refrigerants could be reduced to 3 % with proper design, compared to (12 to 33) % from the experiments. The LLSL-HX improved performance of refrigerants with high molar heat capacity (here, the medium-pressure refrigerants) by (1.0 to 1.5) %. The lower-GWP medium-pressure refrigerants had COP (0.2 to 2.3) % less than R-134a. The lower-GWP high-pressure refrigerants had COP (2.3 to 3.2) % higher than R-410A.

Keywords

air conditioning; CYCLE_D-HX; experimental measurement; heat pump; Low GWP; model; refrigerants.

Table of Contents

List of Figures

List of Tables

Acknowledgments

The authors gratefully acknowledge financial support from the U.S. Department of Defense, Strategic Environmental Research and Development Program (SERDP), project WP 19-F3-1385, with Robin Nissan serving as Project Manager. The authors thank the following NIST staff for their review of this document: Dr. Lingnan Lin, Josh Hughes, Dr. Greg Linteris, Bill Healy, and the NIST editorial board. John Wamsley and Art Ellison are recognized for their construction and maintenance of the test apparatus. Mike Bichnevicius and Patrick Gönner assisted with experimental tests. Mark Kedzierski provided valuable consultation for the statistical regressions.

Author Contributions

Author 1: Conceptualization, Formal analysis, Investigation, Validation, Writing – original draft
Author 2: Conceptualization, Project administration, Methodology, Writing – review & editing;
Author 3: Methodology, Software; **Author 4**: Investigation; **Author 5**: Investigation

1 Introduction

1.1 History of CYCLE_D-HX model

The Montreal Protocol of 1987 [1] spurred the HVAC&R industry's effort to replace chlorinated refrigerants, which were linked to stratospheric ozone destruction [2]. Chlorine-free hydrofluorocarbons (HFCs) and 'natural' refrigerants were top replacement candidates [3]. Methods were needed to evaluate the numerous candidate refrigerants and their mixtures. One option was to screen refrigerants based on their performance at specified evaporator and condenser saturation temperatures ($T_{sat,evap}$, $T_{sat,cond}$) appropriate to the application. However, McLinden & Radermacher [3] showed that different methods of specifying T_{sat} significantly changed the COP estimate, particularly for high-glide mixtures. For example, the COP of R-22/114 varied from 3 to 6 depending on the T_{sat} specification method. To avoid this undesirable uncertainty related to specifying T_{sat}, they proposed the specification of both: (a) temperature profiles of the heat-transfer fluids (HTFs) acting as the heat source and sink, and (b) capacity per total heat exchanger area, Q/A_{total}. These specifications are convenient because HVAC&R equipment requirements typically include capacity, process temperatures, and limited A_{total} because of size or cost constraints. Domanski & McLinden ([4], [5]) accordingly developed a cycle model, CYCLE-11, that took as input the HTF inlet and outlet temperatures and the 'average effective temperature difference' (ΔT_{hx}) in each heat exchanger:

$$\Delta T_{\text{hx}} = Q_{\text{hx}} / UA_{\text{hx}} = Q_{\text{hx}} \left(\sum \frac{Q_{\text{i}}}{\Delta T_{\text{i}}} \right)^{-1} \qquad (1)$$

where Q_i and ΔT_i were the heat transfer and log-mean temperature difference in each heat-exchanger section (e.g., superheated, subcooled, two-phase). The overall heat-transfer coefficient, U, was assumed to be the same in all heat-exchanger (HX) sections. Additional inputs included compressor efficiency and pressure drop in the evaporator and condenser (ΔP_{evap}, ΔP_{cond}). The name CYCLE-11 reflects the eleven primary thermodynamic states considered for a vapor-compression cycle with a liquid-line/suction-line heat exchanger (i.e., LLSL-HX cycle, Fig. 1, Fig. 2). A LLSL-HX, or other throttle-irreversibility-reducing device, should be considered because they can improve the performance of refrigerants with high vapor molar heat capacity ([6], [7]).

Pannock and Didion [8] used CYCLE-11 to evaluate R-22 alternatives. To achieve fixed Q/A_{total} in their experimental validation studies, they used constant evaporator and condenser areas, A_{evap} and A_{cond}, and fixed Q by adjusting compressor speed for each refrigerant. For performance comparison of different refrigerants, they recommended correcting experimental results for differences in compressor efficiency, since differences in refrigerants' volumetric capacity (Q_{vol}) required adjusting the compressor to off-design speeds with sub-optimal performance. Also, differences between the simulations and experiments were partially attributed to the model's lack of refrigerant ΔP and heat-transfer coefficient (HTC) correlations ([8], p. 25, 33). A subsequent model upgrade, CYCLE-11.UA, optionally included these correlations, and took UA_{hx} or ΔT_{hx} as input [9]. Brown et al. [10] used CYCLE-11.UA-CO_2 to compare CO_2 and R134a for mobile air conditioning, using data from [11], [12] as a reference. Brown et al. [13] also used the model to compare CO_2 and R-22 for air conditioners.

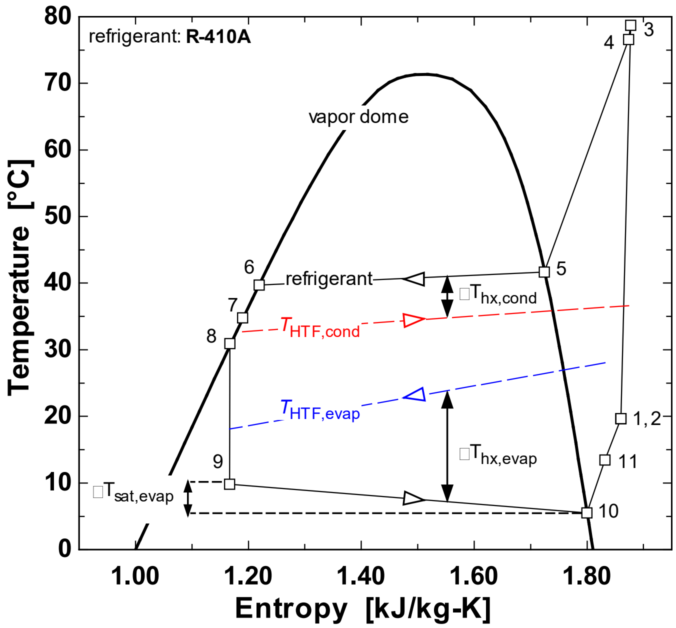

Fig. 1. Temperature-entropy diagram for R-410A in the LLSL-HX cycle.

CYCLE-11.UA was further developed [14] and released as an executable program CYCLE_D-HX [15], [16]. Added features include optional specification of HX tube geometry and circuiting (i.e., number of parallel refrigerant flow paths for a set of tubes), and simulation of advanced cycles. Further, the program can optimize the HX tube circuitry to maximize COP. For example, the number of circuits may be increased to reduce the refrigerant mass flux and ΔP, if the benefit of lower ΔP outweighs the penalty of reduced HTC and leads to improved COP [14]. The model is useful for preliminary refrigerant screening and system design for vapor-compression cycles using tube-based forced-convection HXs. For example, the model was used to evaluate replacements for high global-warming-potential (GWP) refrigerants, whose future use is limited by regional and global regulations [17], [18]. Domanski et al. [19] used CYCLE_D-HX to evaluate low-GWP options for medium and high-pressure applications, and Bell et al. [20] and Domanski et al. [21] used the model to select candidates for non-flammable R-134a replacements, which were later extensively tested in [22]. The referenced simulation-based low-GWP refrigerant screening studies are supported by the experimental validation presented in this work.

1.2 Objectives and overview

The primary objectives of this study were to experimentally validate CYCLE_D-HX and demonstrate its use for fairly comparing refrigerants' potential. We measured performance of R-134a, R-410A, and eight low-GWP candidate replacements for these refrigerants, in a small breadboard heat-pump test apparatus (Section 2). The model was tuned to the test-apparatus hardware using a limited set of tests, and then used to simulate all tests (Section 3.1). The

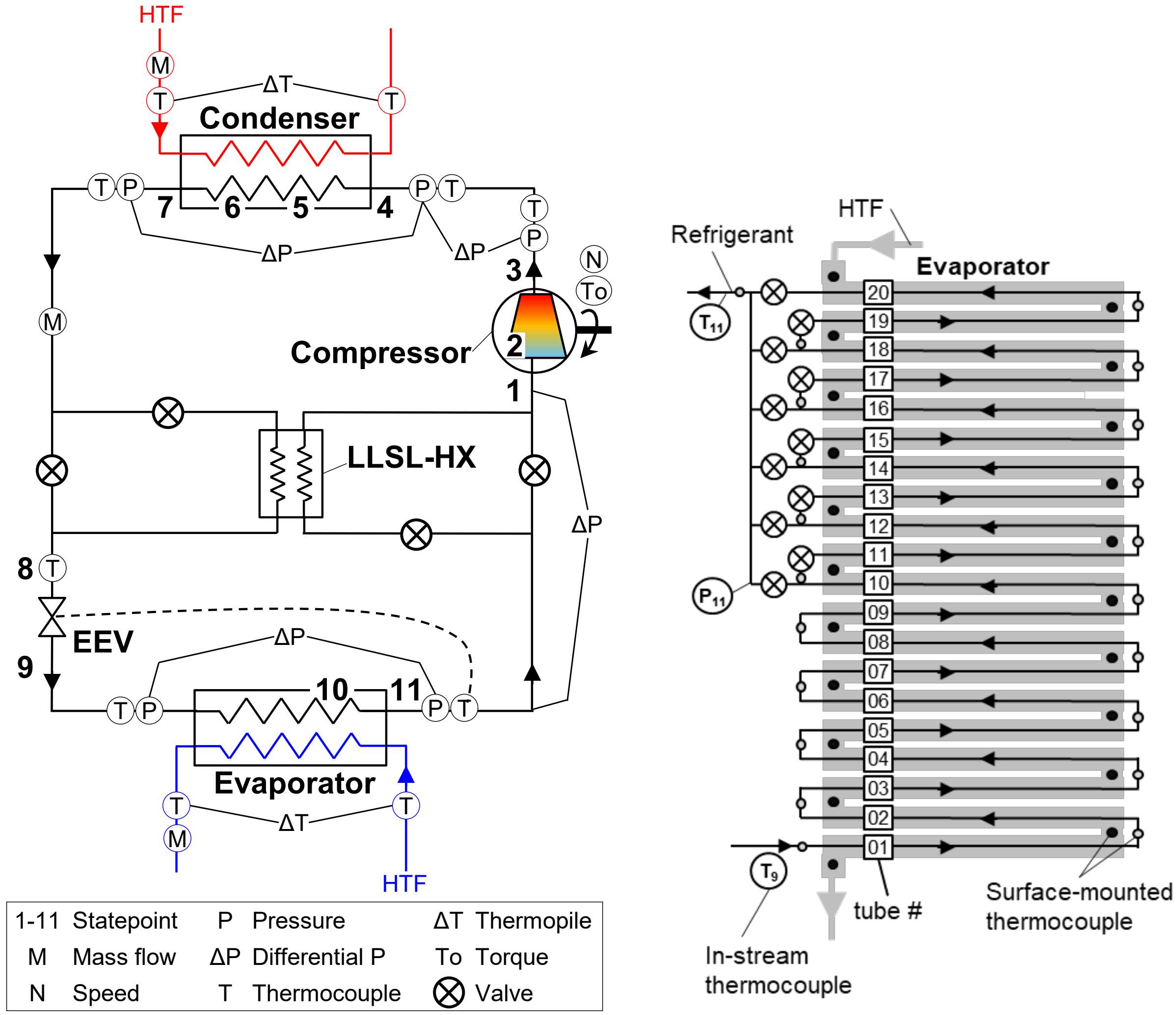

Fig. 2. Test apparatus schematics: (left) entire cycle, (right) evaporator with adjustable number of active tubes.

simulations and experimental measurements were compared to validate model (Section 3.2). Finally, the model was used to compare the refrigerants' performance potential by applying: (1) equal compressor efficiency for all refrigerants, and (2) evaporator and condenser circuitry optimized for each refrigerant (Section 4).

The model is only briefly presented here, for more detail refer to [5], [10], [14], [15]. All data from the experiments and simulations are available at [23]. All refrigerant properties used in this work were calculated using REFPROP [24].

2 Experimental Tests

2.1 Test apparatus

The test apparatus is an extensively-instrumented modular heat-pump system derived from the original set-up used by Pannock and Didion [8] (Fig. 2, Table 1, Table 2). The system uses a variable-speed, oil-lubricated, reciprocating compressor powered by an electric motor and inverter, where the inverter speed controls cooling or heating capacity. The evaporator and condenser are single circuits (i.e., no parallel tube branches). These HX's number of active tubes can be adjusted from 10 to 20 to change the active heat exchange areas (A_{evap}, A_{cond}) and control heat flux and ΔP. The evaporator and condenser are made of copper tubes with annular counter-flow configuration, where the refrigerant flows in the internally-rifled inner tube and the HTF flows in the smooth annular space. An electronic expansion valve (EEV) regulates the evaporator-exit superheat. The refrigerant circuit can be configured for a 'basic cycle' (i.e., LLSL-HX is bypassed), or a 'LLSL-HX cycle' (Fig. 2). A chiller removes heat from the HTF flowing through the condenser, and a circulation heater applies the evaporator load to the HTF flowing through the evaporator. HTF temperatures and flowrates are adjusted to achieve refrigerant-side conditions that emulate typical air-conditioning equipment. A data acquisition system records measurements at 40-second intervals, where the reported values are the averages from a 30-minute steady-state window. Differences in refrigerant- and HTF-side energy transfer measurements in the condenser and evaporator did not exceed 5 %. More details about the test apparatus are in the Appendix and [25].

Table 1. Test apparatus parameters.

Parameter	Value
Compressor: type	reciprocating
Compressor: # cylinders	2
Compressor: displacement (D_{comp})	7.165 cm^3
EEV: orifice diameter	1 mm
HX inner tube: active length	560 mm
HX inner tube: ID	8.46 mm
HX inner tube: OD	9.52 mm
HX inner tube: inner surface	rifled microfin
HX inner tube: material	copper
LLSL-HX: nominal capacity	370 W
LLSL-HX: type	corrugated (liquid side)
LLSL-HX: shell OD	51 mm

Table 2. Measurement uncertainty.

Measurement	±Unc.[a]
M (mass flow)	0.2 %
N (comp. speed)	0.02 Hz
P (pressure)	3.5 kPa
ΔP – condenser	1.5 kPa
ΔP – discharge line [b]	1.0 kPa
ΔP – evaporator	0.8 kPa
ΔP – suction line	0.3 kPa
T - refrig. in-stream	0.06 °C
T – HTF	0.6 °C
T – surface mount [c]	0.6 °C
ΔT (thermopile)	0.015 K
To (comp. torque)	0.037 N m

[a] All uncertainties are for a 95 % confidence interval ($k=2$).

[b] The discharge line pressure drop shown in [23] is $\Delta P = P_3\text{-}P_4$ because the differential measurement was too noisy.

[c] Surface-mounted thermocouples used to measure refrigerant and HTF temperature profile and determine the number of tubes with vapor, liquid, and two-phase refrigerant (Fig. 2). Measurements briefly discussed in [25].

2.2 Test protocol

Ten refrigerants were tested at varied capacity, to evaluate the predictive capability of CYCLE_D-HX over wide-ranging conditions (Table 3). Tested 'medium-pressure' refrigerants included R-134a, and five lower-GWP replacements including: R-1234yf (A2L classification) and four of the 'best' non-flammable candidates from [21], R-513A, R-450A, Tern-1, and R-515B. Tern-1 is a ternary blend developed by NIST for [22]. Tested 'high-pressure' refrigerants included R-410A, and three lower-GWP replacements with 'A2L' safety classification: R-32, R-454B, and R-452B. The medium- and high-pressure refrigerants were respectively tested in two separate groups with different capacity and HX configuration due to limitations of compressor speed, ΔP_{evap}, and $\Delta P_{evap.}$ All tests within a group used the same A_{evap}, A_{cond}, $A_{total}=A_{evap}+A_{cond}$, range of Q, and therefore the same Q/A_{total}.

Table 3. Tested refrigerants.

Refrigerant [a]	Components	Composition mass fraction (%)	Safety group [b]	*NBP* °C	$c_{p,v}$ [c] J mol^{-1} K^{-1}	GWP [d] 100-yr
		Medium-pressure refrigerants				
R-134a	R-134a	100	A1	-26.1	79.7	1300
R-513A	R-134a/1234yf	44.0/56.0	A1	-29.5	85.5	573
R-450A	R-134a/1234ze(E)	42.0/58.0	A1	-22.7	86.9	547
Tern-1	R-134a/1234yf/1234ze(E)	49.2/33.8/17.0	-- [e]	-27.4	85.3	640
R-515B	R-227ea/1234ze(E)	8.9/91.1	A1	-18.8	94.8	299
R-1234yf	R-1234yf	100	A2L	-29.5	90.9	<1
		High-pressure refrigerants				
R-410A	R-32/125	50.0/50.0	A1	-51.4	59.3	1924
R-32	R-32	100	A2L	-51.7	47.4	677
R-454B	R-32/1234yf	68.9/31.1	A2L	-49.5	54.2	467
R-452B	R-32/125/1234yf	67.0/7.0/26.0	A2L	-49.8	54.8	676

[a] All tested refrigerants have zero ozone-depletion potential.

[b] From ANSI/ASHRAE Standard 34 [26]. A = lower toxicity, 1 = no flame propagation, 2L = lower flammability and burning velocity ≤ 10 cm s^{-1}.

[c] Evaluated for saturated vapor at $T = 0.65\ T_{cr}$, per [6].

[d] Mass-weighted values from ([27], p. 732).

[e] Not listed in [26]. Expected rating is A1, per [22].

2.2.1 *R-134a and medium-pressure low-GWP replacements*

The baseline test with R-134a in a basic cycle established the control parameter settings required to reach the operating parameters listed in Table 4. A compressor speed of 13.5 Hz generated 1.5 kW cooling capacity. The HTF inlet temperatures were set to target refrigerant average T_{sat} of 8 °C in the evaporator and 40 °C in the condenser; these temperatures represent typical values we've measured for air-source heat pumps operating at 'Cooling A' conditions [28], i.e. indoor dry-bulb 26.7 °C and wet-bulb 19.4 °C, outdoor dry-bulb 35.0 °C and wet-bulb 23.9 °C.

$$T_{\text{sat,evap}} = \left(T_9 + T_{10}\right)/2 = \left(T_9 + T\left(P_9 - \Delta P_{\text{evap}}, x = 1\right)\right)/2 \tag{2}$$

$$T_{\text{sat,cond}} = \left(T_5 + T_6\right)/2 = \left(T\left(P_7 + \Delta P_{\text{cond}}, x = 1\right) + T\left(P_7, x = 0\right)\right)/2 \tag{3}$$

where T is temperature, P is pressure, x is thermodynamic quality, and the state numbers are shown in Fig. 2. Property calculations using [24] are shown, for example, as $T(P_7, x{=}0)$, which represents calculation of refrigerant saturated liquid temperature at P_7. Evaporator and condenser dewpoint temperature drops (a measure of ΔP):

$$\Delta T_{\text{dew,evap}} = T\left(P_9, x=1\right) - T\left(P_{11}, x=1\right) \tag{4}$$

$$\Delta T_{\text{dew,cond}} = T\left(P_4, x=1\right) - T\left(P_7, x=1\right) \tag{5}$$

of 2 K were targeted. CYCLE_D-HX showed these values were optimal for R-134a since the corresponding mass flux yielded a high HTC but only moderate ΔP penalty. These ΔT_{dew} values were achieved using 10 evaporator tubes and 16 condenser tubes. An evaporator-exit superheat of 15 K was used because it yielded the most repeatable compressor efficiency. (We also found superheat ≥ 8 K improved agreement in refrigerant- and HTF-side energy transfer measurement, likely because it ensured completely superheated refrigerant.) A refrigerant charge of 1420 g produced the targeted subcooling of 5 K. The HTF ΔT targets were 10 K in the evaporator and 4 K in the condenser, and were achieved by adjusting the respective HTF flowrates. The evaporator HTF was a potassium formate brine (Dynalene HC40) whose specific heat was measured and reported in [25], and the condenser HTF was distilled water.

Next, R-134a and the five medium-pressure lower-GWP replacement candidates were tested at varied capacity (Table 5) to quantify performance over a range of heat and mass flux, for a total of 135 tests. The compressor speed was adjusted to reach the primary cooling capacity targets of (1.3, 1.5, and 1.7) kW. Additional tests at higher capacities of (1.9 and 2.0) kW were also performed for R-134a, R-513A, and R-450A, but these test points were abandoned for Tern-1 and R-515B because the refrigerant mass flux and ΔP were too high to represent conditions for a well-designed evaporator and condenser. The refrigerant charge was adjusted for each test to achieve the target subcooling. The other control parameters were fixed for all tests at the values established in the baseline tests. All refrigerants were tested in a basic cycle and a LLSL-HX cycle. For the LLSL-HX cycle, a lower evaporator-exit superheat of 8 K was used, where the LLSL-HX warmed the vapor approximately to the 15 K superheat used for basic-cycle tests. Test conditions were repeated to quantify average performance, and to reduce the 95 % confidence interval (CI, at $k=2$ standard deviations) for the COP vs. capacity regression to about ±1 % (Section 3.2).

Table 4. Operating and control parameters for the R-134a baseline test in a basic cycle.

#	Operating parameter	Value [a]	Control Parameter	Value [a]
1	Cooling capacity [b]	1.499 ± 0.003 kW	Comp. speed	14.44 ± 0.02 Hz
2	Average $T_{sat,evap}$	8.02 ± 0.13 °C	HTF inlet temp: evap.	27.85 ± 0.6 °C
3	Average $T_{sat,cond}$	40.48 ± 0.15 °C	HTF inlet temp: cond.	32.73 ± 0.6 °C
4	$\Delta T_{dew,evap}$	2.55 ± 0.06 K	Number of tubes: evap.	10
5	$\Delta T_{dew,cond}$	1.55 ± 0.05 K	Number of tubes: cond.	16
6	Superheat (evap. out)	15.0 ± 0.3 K	EEV opening [c]	--
7	Subcooling (cond. out)	5.2 ± 0.15 K	Refrigerant charge	1420 ± 20 g
8	HTF ΔT: evap	10.01 ± 0.015 K	HTF flowrate: evap	56.2 ± 0.11 g s^{-1}
9	HTF ΔT: cond	4.00 ± 0.015 K	HTF flowrate: cond	97.7 ± 0.20 g s^{-1}

[a] When provided, ±uncertainty is for 95 % CI ($k = 2$).
[b] Measured on refrigerant side. Uncertainty calculated per [25].
[c] Value wasn't recorded.

Table 5. Test matrix: R-134a and medium-pressure replacements.

Parameter	Unit	Tol.	Target value				
Cooling capacity	kW	±2 %	1.3	1.5	1.7	1.9	2.0
HTF ΔT: evap.	K	±0.02	8.67	10.00	11.33	12.67	13.33
HTF inlet T: cond.	°C	±0.2	32.7	32.7	32.7	32.7	32.7
HTF inlet T: evap.	°C	±0.3	27.9	27.9	27.9	27.9	27.9
HTF flowrate: cond.	g/s	±0.3	97.6	97.6	97.6	97.6	97.6
HTF flowrate: evap.	g/s	±0.3	56.3	56.3	56.3	56.3	56.3
Subcooling: cond. out	K	±0.5	5	5	5	5	5
Superheat: evap. out [a]	K	±1.0	15 (8)	15 (8)	15 (8)	15 (8)	15 (8)
# Tests: R-134a [a]	--	--	7 (6)	7 (6)	6 (6)	4 (4)	3 (2)
# Tests: R-513A [a]	--	--	3 (2)	3 (2)	3 (2)	3 (2)	--
# Tests: R-450A [a]	--	--	4 (3)	4 (3)	4 (3)	1 (0)	--
# Tests: Tern-1 [a]	--	--	4 (3)	4 (3)	4 (3)	--	--
# Tests: R-515B [a]	--	--	4 (3)	4 (3)	4 (3)	--	--
# Tests: R-1234yf [a]	--	--	4 (3)	4 (3)	4 (3)	--	--

[a] Value for tests with the: basic cycle (LLSL-HX cycle).

2.2.2 *R-410A and high-pressure low-GWP replacements*

The R-410A baseline test was similar to the R-134a baseline test but was run at a higher compressor speed of 18.85 Hz to avoid erratic compressor performance, which occurred at lower speeds with high-pressure refrigerants (Table 6). (Compressor speeds ≤13 Hz produced erratic isentropic and volumetric efficiencies, and speeds ≤ 8 Hz would result in insufficient compressor lubrication.) As a result of a higher compressor speed and higher Q_{vol}, the baseline capacity of R-410A was 3.63 kW, much higher than 1.5 kW for the R-134a baseline test. However, the evaporator and condenser HTF inlet temperatures were the same as with R-134a. The number of active evaporator and condenser tubes were increased to 14 and 20 because of the larger heat duty. The evaporator/condenser tube ratio for R-410A (14/20=0.70) was close to that for R-134a (10/14=0.71). This configuration yielded a notably higher $\Delta T_{\mathrm{dew,evap}}$ of 6.05 K (compared to 2.55 K for the R-134a baseline test), but a similar $\Delta T_{\mathrm{dew,cond}}$ of 1.97 K (compared to 1.55 K for the R-134a baseline test). The superheat and subcooling were the same as with R-134a. The HTF ΔT targets were also the same as for R-134a, though they required the HTF flowrates to be increased in proportion to the capacity.

Following the baseline test, R-410A and the three high-pressure low-GWP refrigerants were tested at capacity ranging from (3.05 to 4.05) kW, for a total of 98 tests (Table 7). The test matrix was similar to that for R-134a and the medium-pressure replacements. Most of the control parameters were fixed from the baseline test including: HTF flowrates and inlet temperatures, number of evaporator and condenser tubes, superheat, and subcooling. All refrigerants were tested in a basic and a LLSL-HX cycle.

Table 6. Operating and control parameters for the R-410A baseline test in a basic cycle.

#	Operating parameter	Value [a]	Control Parameter	Value [a]
1	Cooling capacity [b]	3.632 ± 0.006 kW	Comp. speed	18.85 ± 0.02 Hz
2	Average $T_{\mathrm{sat,evap}}$	5.55 ± 0.08 °C	HTF inlet temp: evap.	28.01 ± 0.6 °C
3	Average $T_{\mathrm{sat,cond}}$	40.95 ± 0.06 °C	HTF inlet temp: cond.	32.69 ± 0.6 °C
4	$\Delta T_{\mathrm{dew,evap}}$	6.05 ± 0.03 K	Number of tubes: evap.	14
5	$\Delta T_{\mathrm{dew,cond}}$	1.97 ± 0.02 K	Number of tubes: cond.	20
6	Superheat (evap. out)	15.1 ± 0.15 K	EEV opening [c]	--
7	Subcooling (cond. out)	5.0 ± 0.1 K	Refrigerant charge	1290 ± 20 g
8	HTF ΔT: evap	10.23 ± 0.015 K	HTF flowrate: evap	131.3 ± 0.26 g s^{-1}
9	HTF ΔT: cond	4.11 ± 0.015 K	HTF flowrate: cond	248.8 ± 0.50 g s^{-1}

[a] When provided, ±uncertainty is for 95 % CI (k=2).

[b] Measured on refrigerant side. Uncertainty calculated per [25].

[c] Value wasn't recorded.

Table 7. Executed test matrix: R-410A and high-pressure replacements.

Parameter	Unit	Tol.	Target value		
Cooling capacity	kW	±2 %	3.05	3.55	4.05
HTF ΔT: evap.	K	±0.02	8.67	10.00	11.33
HTF inlet T: evap.	°C	±0.3	27.9	27.9	27.9
HTF inlet T: cond.	°C	±0.2	32.7	32.7	32.7
HTF flowrate: evap.	g/s	±0.6	131.4	131.4	131.4
HTF flowrate: cond.	g/s	±0.6	248.9	248.9	248.9
Superheat: evap. out [a]	K	±1.0	15 (8)	15 (8)	15 (8)
Subcooling: cond. out	K	±0.5	5	5	5
# Tests: R-410A [a,b]	--	--	6 (5)	7 (5)	6 (5)
# Tests: R-32 [a]	--	--	4 (3)	5 (3)	4 (3)
# Tests: R-454B [a]	--	--	4 (3)	4 (3)	4 (3)
# Tests: R-452B [a,b]	--	--	4 (3)	4 (3)	4 (3)

[a] Value for tests with the: basic cycle (LLSL-HX cycle).

[b] In the data processing, we omitted 2(2) [a] medium-capacity tests with R-410A and 2(1) [a] tests with R-452B that occurred after the compressor valves were replaced, because the compressor efficiency at these conditions was significantly higher than for previous tests with the same refrigerants.

3 Validation of CYCLE_D-HX model

3.1 Simulation configuration

All experimental tests were simulated using CYCLE_D-HX. First, four 'Reference Case' experimental data sets were input to the model to calculate 'Reference Parameters' tuned to the test apparatus (Table 8, Table 9). Inputs included LLSL-HX effectiveness, HTF inlet and outlet temperatures, ΔP_{evap}, ΔP_{cond}, superheat, subcooling, evaporator and condenser tube geometry and number of circuits, compressor efficiency, capacity, and ΔT_{dew} in the suction and discharge lines. $\Delta T_{\text{hx,evap}}$ and $\Delta T_{\text{hx,cond}}$, Eq. (1), weren't direct inputs from measurements, but rather were iteratively adjusted until the modeled evaporator inlet (P_9) and condenser outlet (P_7) pressures matched the measurements. The 'Reference Parameters' are evaporator and condenser: (1) combined heat-transfer resistance of the tube wall and HTF (R_{tube} + R_{HTF}) and (2) refrigerant two-phase ΔP multiplication factor, $factor_{\Delta\text{p}}$. In subsequent simulations, the conductance was calculated as:

$$1/UA_{\text{hx}} = R_{\text{hx}} = R_{\text{r}} + \left(R_{\text{tube}} + R_{\text{HTF}}\right) \tag{6}$$

where the refrigerant-side resistance is $R_{\text{r}}=A_{\text{r}}^{-1}h_{\text{r}}^{-1}$, and the refrigerant two-phase HTC, h_{r}, came from correlations [29]–[31]. Also, refrigerant ΔP was calculated as:

$$\Delta P_r = \Delta P_{\text{predicted}} \times factor_{\Delta p} \tag{7}$$

where $\Delta P_{\text{predicted}}$ comes from correlations [32], [33]. All simulations were performed using the same input set as the 'Reference Cases', excluding $\Delta T_{\text{hx,evap}}$, $\Delta T_{\text{hx,cond}}$, ΔP_{evap}, and ΔP_{cond}, since the model calculated these values. The model predicted the cycle thermodynamic states, COP, Q_{vol}, and other 'Outputs' listed in Table 9.

<u>Reference Case: 'R-134a Basic'</u> inputs are from the R-134a baseline test (Table 4), and the associated 'Reference Parameters' were used for simulations of the tests with R-134a and the medium-pressure low-GWP alternatives in the basic cycle. Similarly, <u>Reference Case: 'R-134a LLSL-HX'</u> inputs are from a R-134a test in the LLSL-HX cycle, where the associated 'Reference Parameters' were used for the simulations of the same refrigerants in the LLSL-HX cycle. Separate 'Reference Cases' were needed because the basic-cycle tests used a superheat of 15 K, whereas the LLSL-HX cycle tests used a significantly lower superheat of 8 K. CYCLE_D-HX, as a simplification, estimates the ΔP and HTC in the superheat section based on the values calculated for the two-phase section. The effect of the superheat section is partially corrected for in the 'Reference' (R_{tube} + R_{HTF}) and $factor_{\Delta\text{p}}$. However, the accuracy of this correction diminishes if the superheat is significantly different than that used to establish the 'Reference Parameters'.

The same approach was used for R-410A and the high-pressure low-GWP replacements, where <u>Reference Case: 'R-410A Basic'</u> was based on the R-410A baseline test (Table 6). <u>Reference Case: 'R-410A LLSL-HX'</u> was for the LLSL-HX cycle (Fig. 1).

Table 8. CYCLE_D-HX 'Reference Case' inputs.

		Reference Case:			
		R-134a Basic	R-134a LLSL-HX	R-410A Basic	R-410A LLSL-HX
Parameter [a]	Unit	Value			
LLSL-HX effectiveness	--	0	0.39	0	0.32
Cooling capacity (Q_{evap})	kW	1.50	1.51	3.63	3.53
Evap: HTF temp. in	°C	27.85	28.14	28.01	28.06
Evap: HTF temp. out	°C	17.84	18.14	17.78	18.11
Evap: ΔT_{hx}	K	13.26	12.09	15.47	13.99
Evap: pressure in (P_9)	kPa	406.9	429.1	1047.1	1091.2
Evap: pressure drop (ΔP_{evap})	kPa	33.71	28.51	176.6	143.4
Evap: superheat	K	15.01	8.05	15.09	7.94
Evap: # tubes	--	10	10	14	14
Cond: HTF temp. in	°C	32.73	32.74	32.69	32.70
Cond: HTF temp. out	°C	36.74	36.79	36.80	36.62
Cond: ΔT_{hx}	K	6.17	6.13	7.66	7.32
Cond: pressure out (P_7)	kPa	1008.4	1008.8	2420.4	2408.6
Cond: pressure drop (ΔP_{cond})	kPa	42.80	43.41	117.6	110.2
Cond: subcool	K	5.24	5.18	5.02	4.91
Cond: # tubes	--	16	16	20	20
Comp: isentropic eff. (η_s)	--	0.85	0.87	0.83	0.84
Comp: volumetric eff. (η_v)	--	0.83	0.84	0.81	0.81
$\Delta T_{dew,suc}$: suction line	°C	0.78	0.85	1.09	1.01
$\Delta T_{dew,dis}$: discharge line	°C	0.64	0.65	0.75	0.77
Test # [b]		677	657	873	877

[a] Other model inputs: Heat exchanger type = counter, Tube inner surface = enhanced, Tube inner diameter = 8.46 mm, Tube length = 558.8 mm, Number of circuits = 1, Electric motor efficiency = 1, Auxiliary Power = 0 kW.

[b] Test # is the sequential test number, and corresponds to value shown in [23].

Table 9. CYCLE_D-HX 'Reference Case' outputs.

		Reference Case:			
		R-134a Basic	R-134a LLSL-HX	R-410A Basic	R-410A LLSL-HX
Parameter	Unit	Value			
COP	--	5.87	6.46	4.44	4.97
Q_{vol}	kJ m^{-3}	2767	2978	5297	5824
Mass flux	kg m^{-2} s^{-1}	158.7	158.7	355.5	344.1
Evap: average T_{sat}	°C	8.15	10.00	5.75	7.8
Evap: glide (T_9-T_{10})	°C	2.6	2.1	6.0	4.6
Evap: R_r	°C kW^{-1}	1.327	1.368	0.502	0.519
Evap: $R_{tube} + R_{HTF}$	°C kW^{-1}	7.513	6.639	3.760	3.444
Evap: UA_{hx}	kW °C^{-1}	0.113	0.125	0.235	0.252
Evap: heat flux (Q/A_r)	kW m^{-2}	10.1	10.2	17.5	17.0
Evap: factor$_{\Delta p}$	--	2.491	2.331	4.131	3.940
Cond: average T_{sat}	°C	40.50	40.50	40.95	40.7
Cond: glide (T_5-T_6)	°C	1.6	1.6	2.1	2.0
Cond: R_r	°C kW^{-1}	1.333	1.334	0.530	0.541
Cond: $R_{tube} + R_{HTF}$	°C kW^{-1}	2.182	2.182	1.192	1.186
Cond: UA_{hx}	kW °C^{-1}	0.285	0.284	0.581	0.579
Cond: heat flux (Q/A_r)	kW m^{-2}	7.4	7.3	15.0	14.3
Cond: $factor_{\Delta p}$	--	5.677	5.765	6.071	5.974
Test # [a]		677	657	873	877

[a] Test # is the sequential test number, and corresponds to value shown in [23].

3.2 Experimental results and model validation

The experimental results and model predictions were compared to validate CYCLE_D-HX. All performance metrics were correlated to capacity (Q_{evap}) by regression using 1st or 2nd order polynomials. The figures in this section show individual experimental data points as symbols (e.g., ●,▲,■), regression (i.e., fit) of experimental data as short-dashed lines (-----), and regression of model predictions as solid lines (——). All data and fits are shown normalized by the regression of experimental data for R-134a or R-410A.

It's critical to note the purpose of the experimental measurements is to validate CYCLE_D-HX, rather than to show the refrigerants' absolute performance potential. The compressor and HX circuitry were configured to maximize the COP with R-134a in the 'baseline test', and this configuration produced sub-optimal performance for other refrigerants. So despite testing the refrigerants with equal Q_{evap}/A_{total} per the recommendation of [3], the comparison wasn't strictly fair. The simulations in Section 4 consider systems with equal compressor efficiency and HX tube circuitry optimized for each refrigerant, and therefore are a fairer comparison of the refrigerants' maximum performance potential. We assume that if the model can correctly predict the experimental test results, the conclusions from the simulations in Section 4 are valid.

The primary performance metrics are:

$$\mathrm{COP} = Q_{\mathrm{evap}} / W_{\mathrm{comp}} = \left(i_{11} - i_9\right) / \left(i_3 - i_1\right) \tag{8}$$

$$Q_{\mathrm{vol}} = Q_{\mathrm{evap}} / \left(v_1 m_r\right) = \left(i_{11} - i_9\right) / v_1 \tag{9}$$

where i_{11} and i_9 are the evaporator outlet and inlet enthalpies, i_3 and i_1 are the compressor discharge and suction enthalpies, v_1 is the suction specific volume, m_r is the refrigerant mass flow. The experimental thermodynamic states were calculated per ([25], Section 3.1).

The compressor isentropic and volumetric efficiencies are:

$$\eta_\mathrm{s} = \frac{i\left(P_3, s_1\right) - i_1}{i_3 - i_1} \tag{10}$$

$$\eta_\mathrm{v} = \frac{m_r v_1}{D_{\mathrm{comp}}\, N} \tag{11}$$

where $i(P_3,s_1)$ is the compressor discharge enthalpy for isentropic compression, N is the compressor speed, and D_{comp} is the compressor displacement (Table 1).

3.2.1 *R-134a and medium-pressure low-GWP replacements*

<u>*Experimental test results*</u>

The experimentally measured COP of R-134a in the basic cycle varied from (7.36 to 3.09) ± 0.5 % as the capacity varied from (1.24 to 2.00) ± 0.0035 kW (Fig. 3). All other medium-pressure refrigerants had lower COP than R-134a. In order of descending COP, they were: Tern-1 and R-513A (they were about the same), R-450A, R-1234yf, and R-515B. Fig. 3 shows the 95 % confidence intervals of the experimental COP vs. capacity curve fit with long-dashed lines (— — —). Where the confidence intervals of two refrigerants overlap, the average performances have no statistically significant difference.

Fig. 4 shows the COPs from Fig. 3 normalized by the curve fit to the R-134a experimental values. The 95 % confidence intervals for the normalized experimental curve fits are approximately ±2 % (not shown). The experimental R-134a regression normalized by itself has a constant value of '1'. Compared to R-134a, the other refrigerants' COPs were: (5 to 6) % lower for Tern-1 and R-513A, (6 to 13) % lower for R-450A, (10 to 15) % lower for R-1234yf, and (13 to 33) % lower for R-515B.

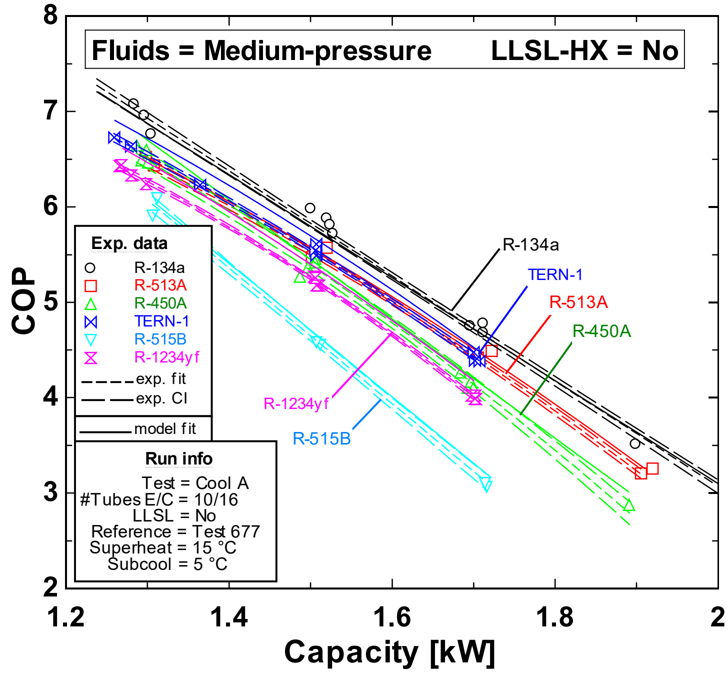

Fig. 3. Measured and predicted COP for medium-pressure refrigerants in the basic cycle.

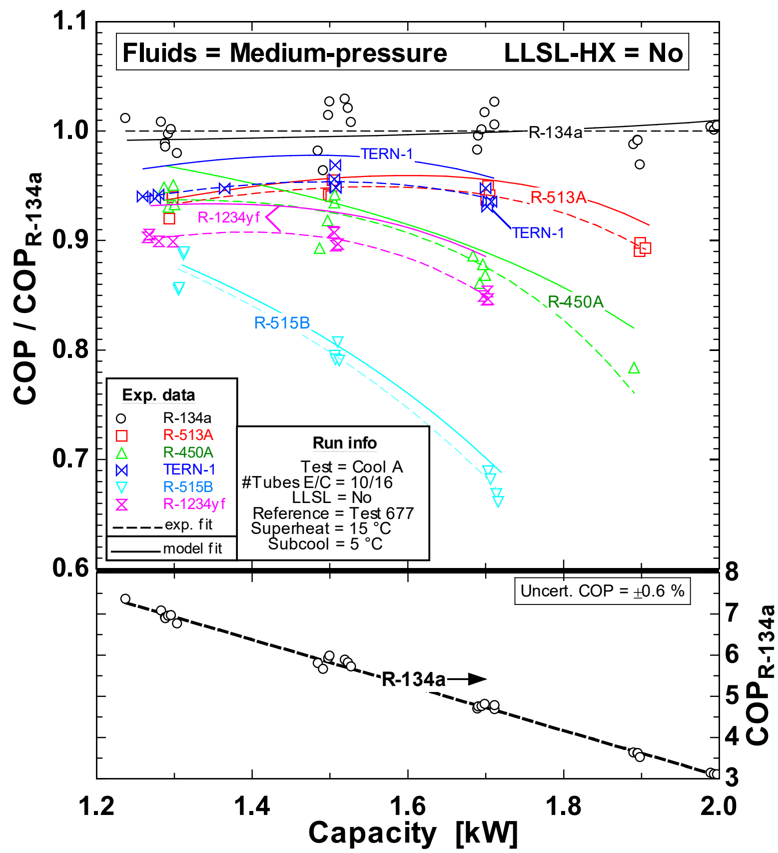

Fig. 4. Measured and predicted COP for medium-pressure refrigerants in basic cycle: (top) normalized by regression of R-134a measurements, (bottom) R-134a measurements.

The Q_{vol} of R-134a ranged (3.2 to 1.8) kJ/m^3 for the basic-cycle tests (Fig. 5). Compared to R-134a the other refrigerants' Q_{vol} was: 3 % higher to 2 % lower for R-513A, (3 to 5) % lower for Tern-1, (5 to 10) % lower for R-1234yf, (15 to 20) % lower for R-450A, and (30 to 40) % lower for R-515B.

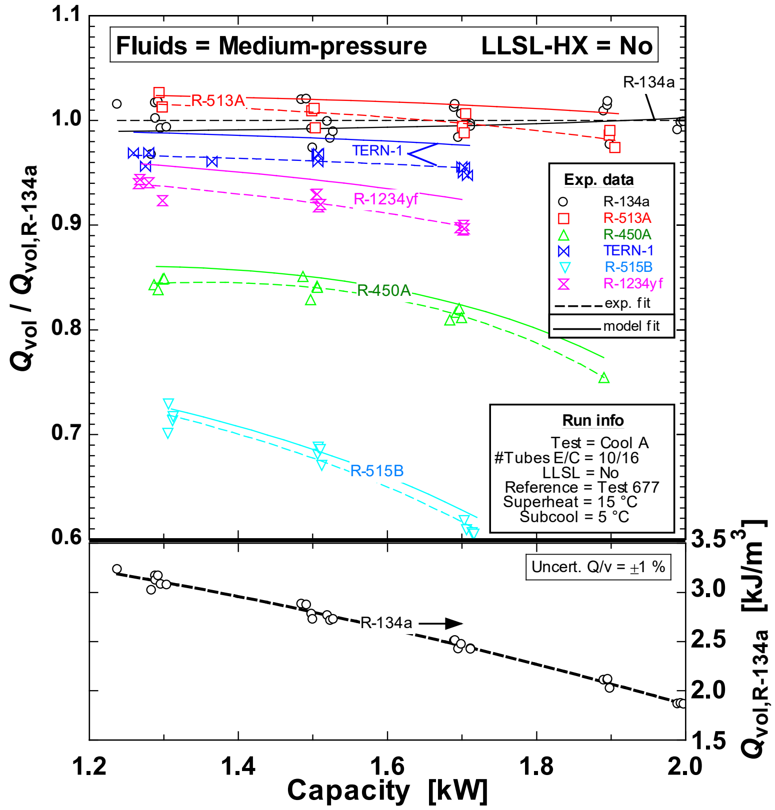

Fig. 5. Measured and predicted volumetric capacity for medium-pressure refrigerants in the basic cycle: (top) values normalized by regression of R-134a measurements, (bottom) R-134a measurements.

The R-134a ΔP_{evap} ranged (20 to 80) kPa (Fig. 6) for the basic-cycle tests. Compared to R-134a, the other refrigerants' ΔP_{evap} was: (10 to 20) % higher for R-513A and Tern-1, (20 to 30) % higher for R-450A, (30 to 50) % higher for R-1234yf, and (50 to 60) % higher for R-515B. The R-134a ΔP_{cond} ranged (30 to 80) kPa. Compared to R-134a the other refrigerants' ΔP_{cond} was: (5 to 15) % higher for R-513A and Tern-1, (5 to 20) % higher for R-450A, (20 to 30) % higher for R-1234yf, and (30 to 45) % higher for R-515B.

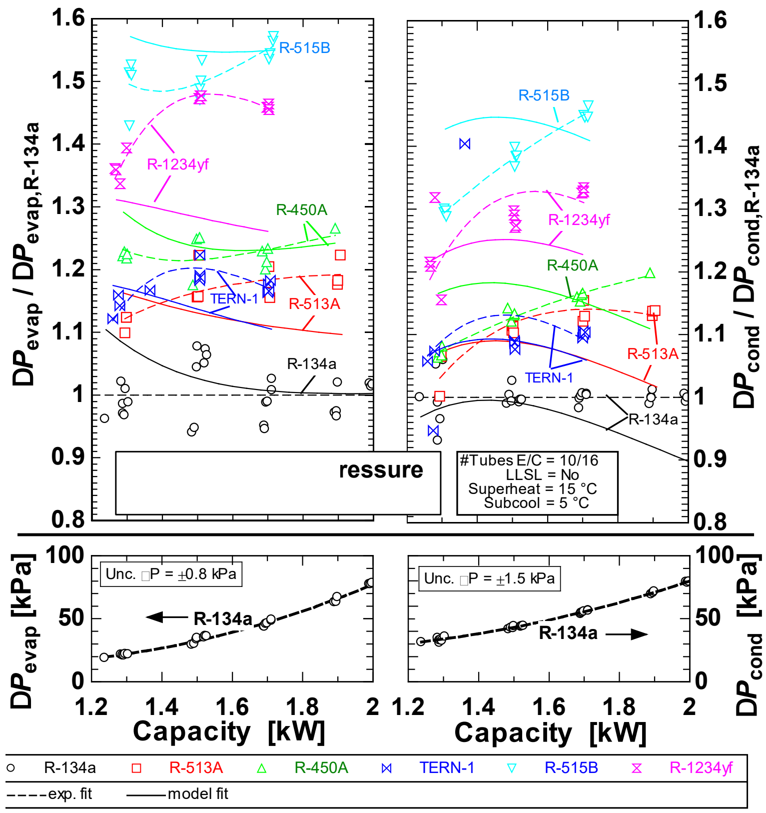

Fig. 6. Measured and predicted pressure drop for medium-pressure refrigerants in the basic cycle: (left) evaporator, (right) condenser, (top) values normalized by regression of R-134a measurements, (bottom) R-134a measurements.

The LLSL-HX cycle performance parameters, COP (Fig. 7), Q_{vol} (not shown), and ΔP (not shown), were normalized by the regression of R-134a experimental measurements in the LLSL-HX cycle. The normalized values were similar to those from the basic cycle.

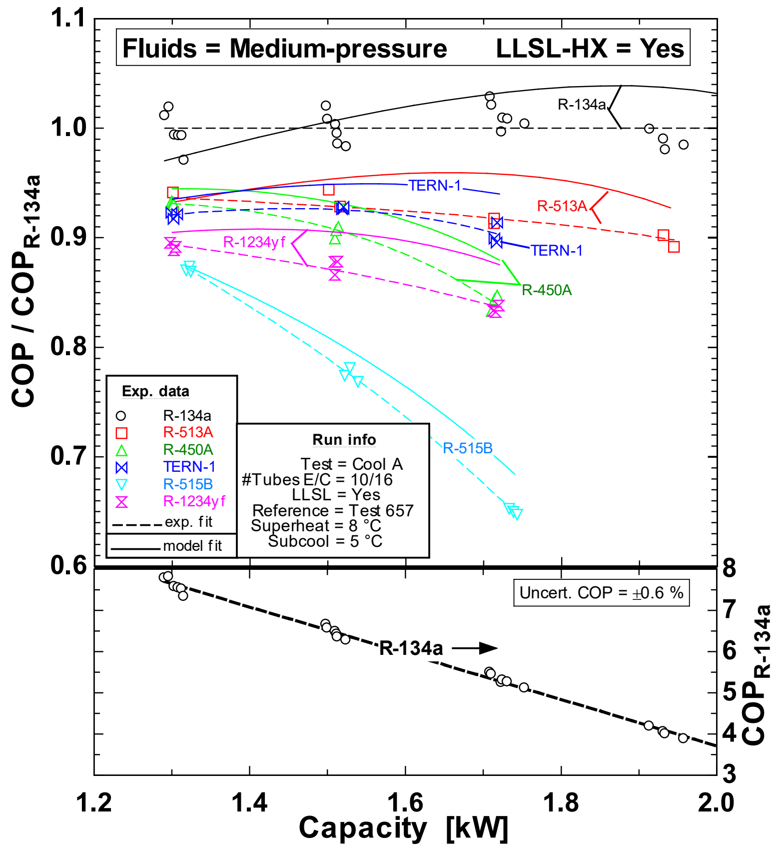

Fig. 7. Measured and predicted COP for medium-pressure refrigerants in the LLSL-HX cycle: (top) values normalized by regression of R-134a measurements, (bottom) R-134a measurements.

The lower COPs of R-1234yf, R-450A, and R-515B are largely attributed to 'hardware effects', rather than inherent refrigerant characteristics. These refrigerants have lower Q_{vol} (Fig. 5) than R-134a (which the test apparatus was optimized for), and sometimes lower compressor volumetric efficiency (Fig. 8), so they required higher compressor speeds to achieve the Q_{evap} target (Table 10). Higher compressor speeds increased the frictional losses, which reduced the isentropic efficiency (Fig. 8) and COP. The refrigerants also had larger ΔP_{evap} and ΔP_{cond}, since they operated at lower pressure and density, and therefore higher velocity (Fig. 6). Higher ΔP required additional compressor power. Further, the ΔP caused a drop in T_{sat} that was unfavorable to efficient countercurrent heat exchange with the HTF [14]. Here, the ΔP and associated ΔT_{sat} were particularly large in the evaporator. The degrading 'hardware effects' unfairly prejudice the COP of these refrigerants since the degradation could be mitigated through proper compressor design and optimizing refrigerant tube circuitry to reduce ΔP. In Section 4, these corrections were applied to more fairly compare the refrigerants' maximum potentials.

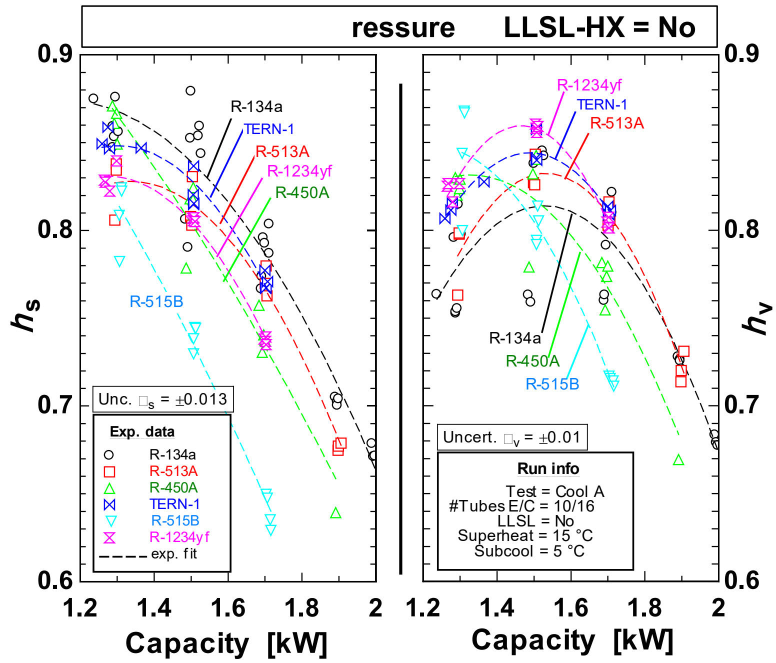

Fig. 8. Measured compressor isentropic efficiency (left) and volumetric efficiency (right), for medium-pressure refrigerants in the basic cycle.

Table 10. Compressor speeds: R-134a and medium-pressure replacements.

Refrigerant	Compressor Speed [Hz] [a]
R-134a	11 to 19
Tern-1	11 to 20
R-513A	12 to 19
R-1234yf	12 to 22
R-450A	13 to 24
R-515B	16 to 37

[a] more detail in ([22], Section 3.3).

Model validation

For the basic-cycle tests, the model-predicted COP and Q_{vol} values (Fig. 4, Fig. 5) were within the confidence intervals (not shown, about ±2 % around the experimental curve fit). For the LLSL-HX cycle tests, CYCLE_D-HX overpredicted the COP (and Q_{vol}, not shown) by (0 to 5) % (Fig. 7). These discrepancies were larger than those for the basic cycle, but the model still ranked the refrigerant COPs the same as the experimental tests.

Differences between the test data and the CYCLE_D-HX predictions are primarily attributed to the refrigerant HTC and ΔP in the condenser and evaporator, since the thermodynamic property data for the tested refrigerants are well established and the other hardware performance parameters are input to the model based on each experimental test (Section 3.1). In cases where the ΔP was well predicted (i.e., within ±10 %), overpredicted

$T_{sat,evap}$ indicated underprediction of $\Delta T_{hx,evap}$, which implied an underestimation of $R_{hx,evap}$, Eqs. (1) and (6). ($R_{HTF} + R_{tube}$) is an unlikely source of error because it was empirically determined (Table 8) and the HTF flow and tube geometry were fixed. So, in these cases, we infer the culprit was an underpredicted $R_{r,evap}$, due to overpredicted refrigerant flow-boiling HTC. Similarly, an underprediction of $T_{sat,evap}$ can indicate an underprediction of refrigerant flow-boiling HTC. In a few cases, we make analogous conclusions about the refrigerant two-phase convection HTC in the condenser and $T_{sat,cond}$.

Detailed comparison of simulations and experimental data:

- **R-134a:** The model predicted the experimental COP and Q_{vol} within ±1 % (Fig. 4). The ΔP_{evap} was overpredicted by 10 % at 1.3 kW capacity (Fig. 6), which caused underprediction in COP. The ΔP_{cond} was underpredicted by 10 % at 2 kW capacity causing the slight overprediction in COP. The $T_{sat,evap}$ and $T_{sat,cond}$ were well predicted, within ±0.2 °C (Fig. 9).
- **R-513A:** The model-predicted COP was (0.5 to 2) % over the experimental values (Fig. 4). The ΔP_{evap} and ΔP_{cond} were predicted within ±3 % at 1.3 kW capacity and were underpredicted by (10 to 15) % at 1.9 kW (Fig. 6). The ΔP discrepancy at higher capacity explains the higher COP discrepancy. The remaining offset in COP prediction was attributed to an overpredicted evaporator HTC, since $T_{sat,evap}$ was overpredicted by about 0.5 °C, whereas the $T_{sat,cond}$ was predicted within ±0.2 °C (Fig. 9).
- **Tern-1:** The model-predicted COP was 3 % over the experimental values (Fig. 4). The ΔP_{evap} and ΔP_{cond} were predicted within ±5 % (Fig. 6). The model overprediction of COP was attributed to an overpredicted evaporator HTC, since $T_{sat,evap}$ was overpredicted by (0.5 to 1) °C, whereas the model nearly exactly predicted $T_{sat,cond}$ (Fig. 9).
- **R-450A:** The model-predicted COP was (1 to 3) % higher than the experimental values (Fig. 4). The ΔP_{evap} and ΔP_{cond} were respectively overpredicted by 5 % and 10 % at 1.3 kW capacity, and nearly exactly predicted at 1.7 kW capacity (Fig. 6). Despite the ΔP overprediction at 1.3 kW, the COP prediction was still 3 % too high. The discrepancy could be explained by overprediction of both evaporator and condenser HTC, since the model overpredicted $T_{sat,evap}$ and underpredicted $T_{sat,cond}$ (Fig. 9). However, the evaporator HTC is the likely culprit since the trend of COP discrepancy closely tracks the trend of $T_{sat,evap}$ discrepancy.
- **R-1234yf:** The model-predicted COP was 3 % higher than the experimental values (Fig. 4). The ΔP_{evap} was underpredicted by 4 % at 1.3 kW capacity, and the overprediction grew to 20 % at 1.7 kW capacity (Fig. 6). The ΔP_{cond} underprediction grew from 0 % to 10 % as the capacity increased from 1.3 kW to 1.7 kW. However, the trend of ΔP discrepancy growth didn't correlate to the trend of nearly constant 3 % COP underprediction. The $T_{sat,evap}$ was underpredicted by a constant ≈1 °C, whereas the $T_{sat,cond}$ prediction was nearly perfect (Fig. 9). Therefore, the COP overprediction was attributed to overprediction of the evaporator HTC.

- **R-515B:** The model-predicted COP was (1 to 2) % larger than the experimental values (Fig. 4). The COP overprediction occurred despite the (0 to 15) % overprediction in ΔP_{evap} and ΔP_{cond} (Fig. 7). The $T_{sat,evap}$ was overpredicted and $T_{sat,cond}$ was underpredicted (Fig. 9), so the COP overprediction was caused by overpredicted HTC in the evaporator and/or condenser.

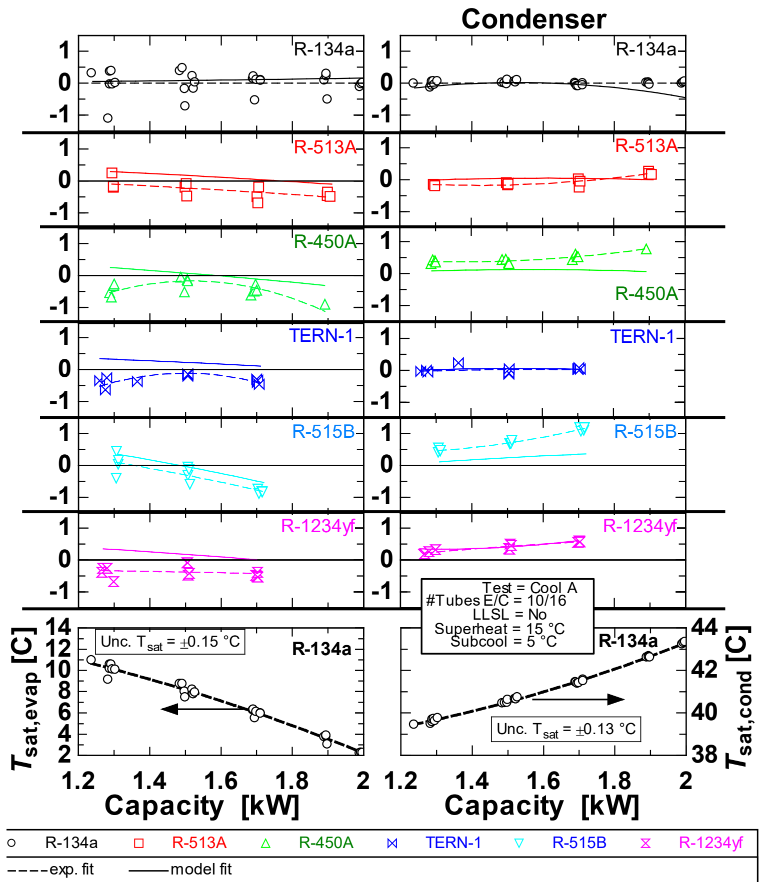

Fig. 9. Measured and predicted average saturation temperatures for medium-pressure refrigerants in the basic cycle: (left) evaporator, (right) condenser, (top) values normalized by regression of R-134a measurements, (bottom) R-134a measurements.

3.2.2 *R-410A and high-pressure low-GWP replacements*

Experimental test results

Fig. 10 shows the COP for the high-pressure refrigerants in basic cycle, normalized by the curve fit to the R-410A experimental values. The COP of R-410A varied from (5.35 to 3.47) ± 0.5 % as the capacity varied from (3.06 to 4.03) ± 0.006 kW. Compared to R-410A, the other refrigerants' COPs were: 3 % higher for R-454B and R-452B, and (10 to 28) % higher for R-32. The higher COPs for R-454B, R-452B, and R-32 were in part because of the lower ΔP (Fig. 12) and higher compressor isentropic efficiency (Fig. 13). R-32 had a particularly high COP at 4.05 kW, about 27 % higher than R-410A (Fig. 10). At this test condition, the R-32 Q_{vol} was much larger than the other refrigerants (23 % higher than R-410A, Fig. 11), so the compressor could achieve the target capacity at a lower speed that had higher isentropic efficiency.

The Q_{vol} of R-410A ranged (6.4 to 4.5) kJ/m^3 for the basic cycle (Fig. 11). Compared to R-410A, the other refrigerants' Q_{vol} was: (1 to 5) % lower for R-454B and R-452B, and (11 to 23) % higher for R-32. The compressor speed ranges were (14 to 21) Hz for R-32, and (14 to 27) Hz for R-410A, R-454B, and R-454B. These ranges were similar for the medium-pressure refrigerants, but the capacity was much larger for the high-pressure refrigerants because they had larger Q_{vol}.

Fig. 12 shows the R-410A ΔP_{evap} ranged (110 to 240) kPa for the basic cycle. Compared to R-410A the other refrigerants' ΔP_{evap} was: (6 to 11) % lower for R-454B and R-452B, and (35 to 40) % lower for R-32. The R-410A ΔP_{cond} ranged (75 to 150) kPa). Compared to R-410A the other refrigerants' ΔP_{cond} was (10 to 13) % lower for R-454B and R-452B, and about 30 % lower for R-32.

The LLSL-HX cycle performance parameters, COP, Q_{vol}, and ΔP, were normalized by the regression of R-410A experimental measurements in the LLSL-HX cycle; the normalized values (not shown) were similar to those from the basic cycle.

Model validation

For the basic cycle, the model-predicted COP and Q_{vol} values for R-410A and R-32 were within the confidence intervals (not shown, about ±2 % around the experimental curve fit) (Fig. 10, Fig. 11). The model overpredicted the COP for R-454B and R-452B by about 3 %. The model ranked the refrigerant COPs the same as the experimental tests. Similar agreement was observed for the LLSL-HX cycle data (not shown).

Detailed comparison of simulations and experimental data:

- **R-410A:** The model predicted the experimental COP and Q_{vol} within ±1.5 % (Fig. 10). The ΔP_{evap} was predicted within ±2 % (Fig. 12). ΔP_{cond} was overpredicted by 6 % at 3.1 kW capacity and underpredicted by 4 % at 4.05 kW capacity; consequently, the COP was respectively underpredicted and overpredicted at these capacities. The $T_{sat,cond}$ was almost exactly predicted, and $T_{sat,evap}$ was predicted within ±0.25 °C (Fig. 14).
- **R-32:** The model underpredicted the experimental COP by (1.0 to 1.5) % (Fig. 10). The ΔP_{evap} was overpredicted by (2 to 4) %, and ΔP_{cond} was predicted within ±3 % (Fig. 12). The small COP underprediction can be partially explained by overpredicted ΔP_{evap}. The remaining COP discrepancy was attributed to a slightly underpredicted condenser HTC, since $T_{sat,cond}$ was overpredicted by about 0.25 °C, whereas the $T_{sat,evap}$ was well predicted, within ±0.1 °C (Fig. 14).
- **R-454B and R-452B:** The model-predicted COP was 3 % over the experimental values (Fig. 10). The ΔP_{evap} was underpredicted slightly, by 3 %. The ΔP_{cond} was overpredicted 10 % at 3.05 kW capacity, and underpredicted 1 % at 4.05 kW capacity (Fig. 12). $T_{sat,evap}$ was overpredicted by about 0.5 °C and $T_{sat,cond}$ was underpredicted by 0.5 °C (Fig. 14). The trend of constant COP overprediction is consistent with the trends in T_{sat}, rather than trends in ΔP prediction, so the error was attributed to overprediction of the HTC in the evaporator and/or condenser.

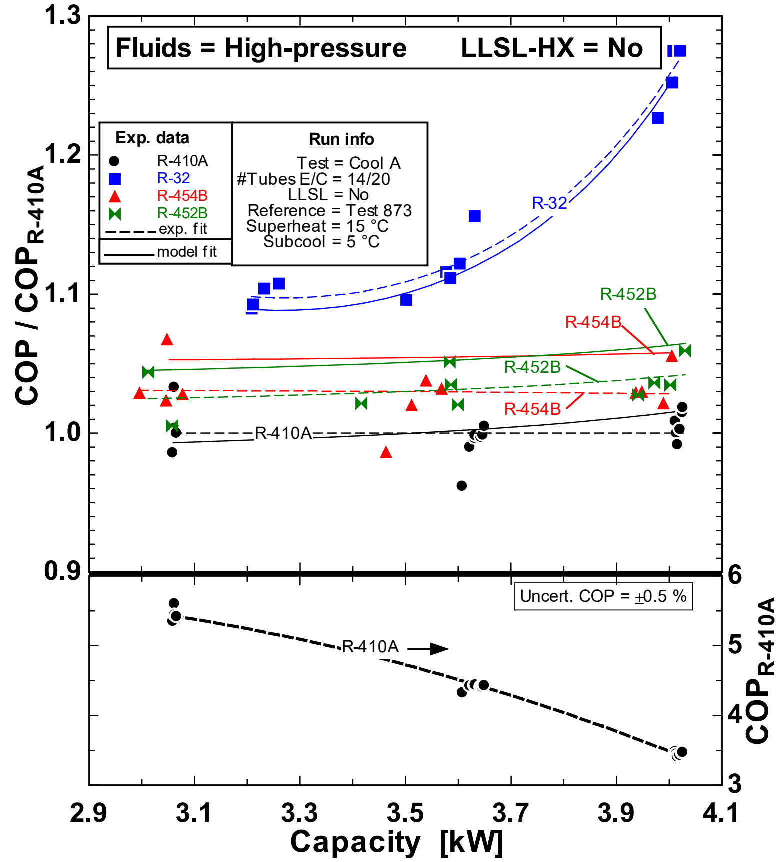

Fig. 10. Measured and predicted COP for high-pressure refrigerants in the basic cycle: (top) values normalized by regression of R-410A measurements, (bottom) R-410A measurements.

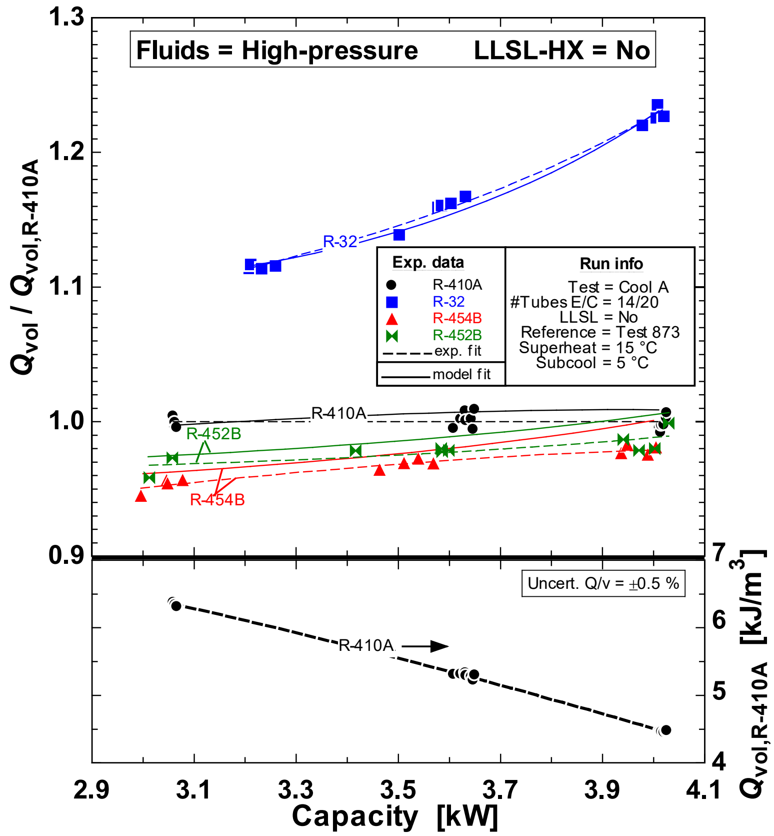

Fig. 11. Measured and predicted volumetric capacity for high-pressure refrigerants in the basic cycle: (top) values normalized by regression of R-410A measurements, (bottom) R-410A measurements.

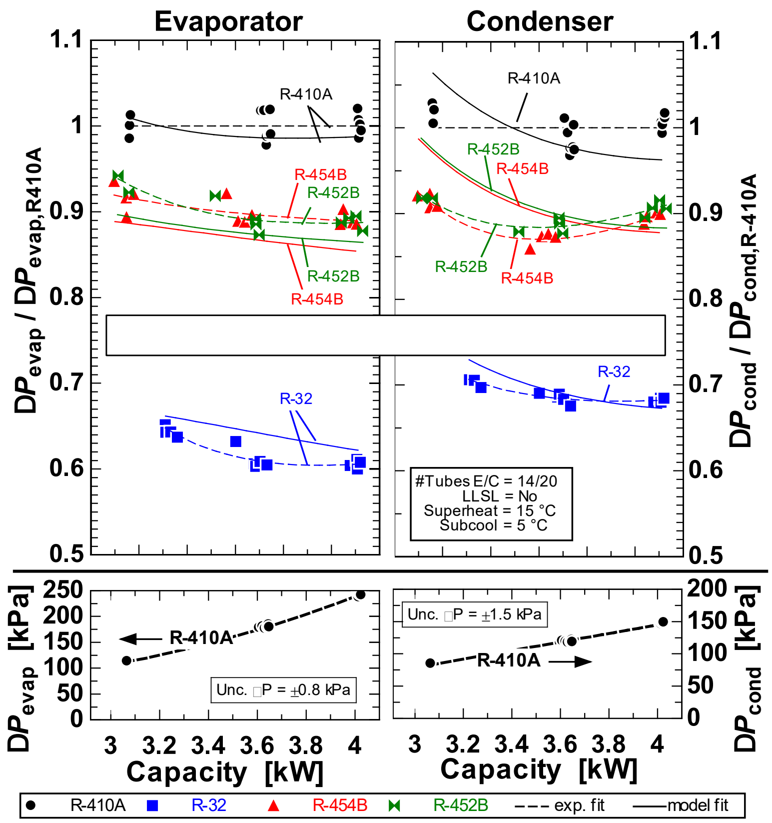

Fig. 12. Measured and predicted pressure drop for high-pressure refrigerants in the basic cycle: (left) evaporator, (right) condenser, (top) values normalized by regression of R-410A measurements, (bottom) R-410A measurements.

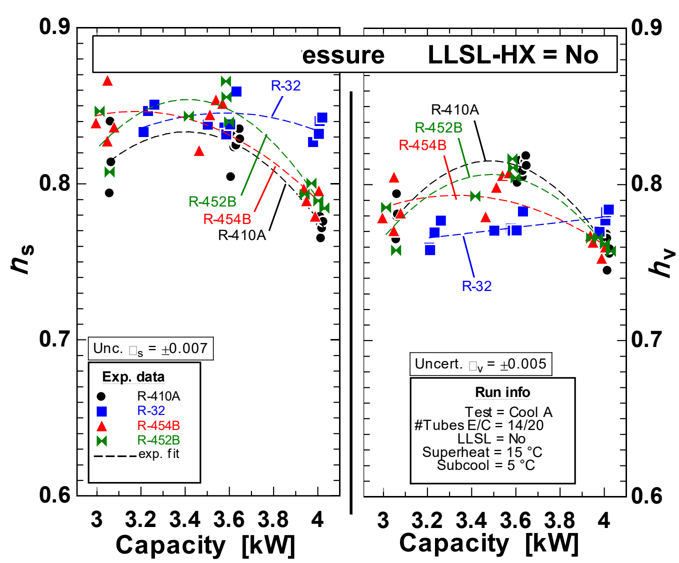

Fig. 13. Measured compressor isentropic efficiency (left) and volumetric efficiency (right), for high-pressure refrigerants in the basic cycle.

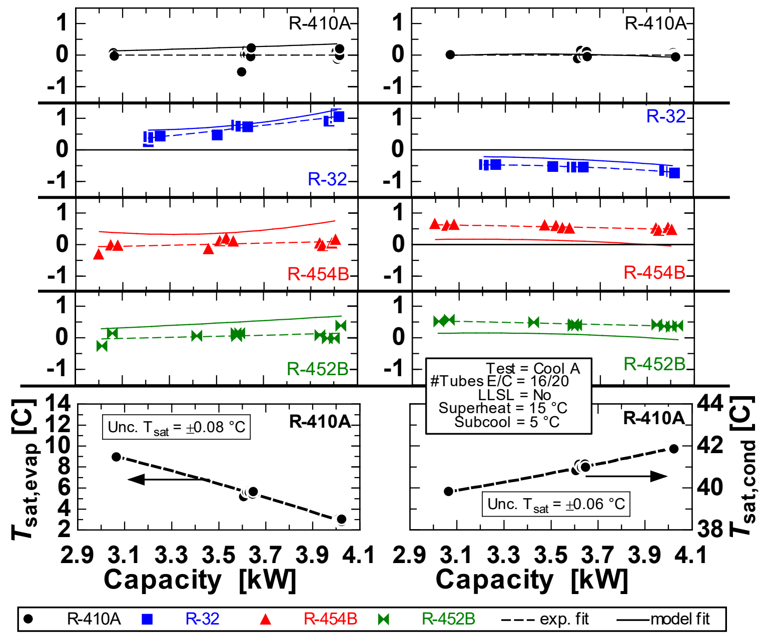

Fig. 14. Measured and predicted average saturation temperatures for high-pressure refrigerants in the basic cycle: (left) evaporator, (right) condenser, (top) values normalized by regression of R-410A measurements, (bottom) R-410A measurements.

4 Simulation of refrigerants' maximum performance potentials

4.1 Simulation configuration

Simulations were performed to compare the maximum performance potentials of the refrigerants in the test apparatus. All refrigerants were simulated at the lower-capacity test conditions for the medium-pressure refrigerants (Table 11). These simulations enabled direct comparison between medium- and high-pressure refrigerants, which wasn't possible in the test apparatus. Three configurations were simulated:

- *Configuration 1: Equal compressor efficiency, basic cycle.*
- *Configuration 2: Equal compressor efficiency, basic cycle, optimized tube circuitry.*
- *Configuration 3: Equal compressor efficiency, LLSL-HX cycle, optimized tube circuitry.*

where the maximum performance potential of each refrigerant is the COP from *Configuration 2 or 3,* whichever is better.

The compressor efficiencies for all refrigerants were set equal to those from the regression of the R-134a experimental measurements (Fig. 8); we assume this is achievable with compressors designed specifically for each refrigerant. When implemented, the tube circuitry optimization was applied to both the evaporator and condenser. When included, the LLSL-HX effectiveness was 0.4, approximately the average from all the tests. The HTF inlet temperatures, superheat, and subcooling values were based on the R-134a baseline test (Table 4). The HTF temperature change was computed as $\Delta T_{\mathrm{HTF}} = Q/(m_{\mathrm{HTF}}\, c_{\mathrm{p,HTF}})$, where $m_{\mathrm{HTF}}\, c_{\mathrm{p,HTF}}$ is the HTF capacitance calculated from the R-134a baseline test (Table 11). The Q_{cond} varied with every refrigerant and test condition, so $\Delta T_{\mathrm{HTF,cond}}$ was adjusted accordingly. In contrast, Q_{evap} and $\Delta T_{\mathrm{HTF,evap}}$ were the same for every refrigerant. Lastly, $\Delta T_{\mathrm{dew,suc}}$ and $\Delta T_{\mathrm{dew,dis}}$ came from the regression of the R-134a experimental data (not shown). The imposed equal Q_{evap}, A_{hx}, and compressor efficiencies for all refrigerants approached the ideal comparison proposed by [3].

All refrigerants were also simulated at the higher-capacity test conditions from the high-pressure refrigerants (Table 12). As with the lower-capacity simulations, we applied equal compressor efficiency, optionally optimized tube circuitry, and optionally included the LLSL-HX. The simulations allowed evaluation of the medium-pressure refrigerants at the high-pressure refrigerant capacity range test conditions, which couldn't be done experimentally since the medium-pressure refrigerants would have had excessive ΔP and would have required compressor speeds above the maximum value for the compressor. Like the lower-capacity tests discussed in the preceding paragraph, the compressor efficiencies, HTF capacitance, $\Delta T_{\mathrm{dew,suc}}$, and $\Delta T_{\mathrm{dew,dis}}$ were based on values from R-410A tests.

Table 11. Inputs for simulations with optimized tube circuitry at the low-capacity range.

Parameter	Unit	Value		
Cooling capacity (Q_{evap})	kW	1.3	1.5	1.7
Comp. isen. eff. (η_s)	--	0.87	0.84	0.79
Comp. vol. eff. (η_v)	--	0.78	0.81	0.80
LLSL-HX effectiveness [a]	--	0 (0.4)	0 (0.4)	0 (0.4)
HTF ΔT: evap.[b]	K	8.68	10.01	11.34
HTF ΔT: cond.[c,d]	K	3.40	4.01	4.68
HTF inlet T: evap.	°C	27.85	27.85	27.85
HTF inlet T: cond.	°C	32.73	32.73	32.73
Number of tubes: evap.	--	10	10	10
Number of tubes: cond.	--	16	16	16
Superheat: evap. out	K	15	15	15
Subcooling: cond. out	K	5	5	5
$\Delta T_{dew,suc}$: suction line	°C	0.47	0.71	1.24
$\Delta T_{dew,dis}$: discharge line	°C	0.56	0.60	0.65

[a] Value for simulations with the: basic cycle (LLSL-HX cycle).
[b] Value based on cooling capacity, and evaporator HTF capacitance 0.1499 kW K^{-1} from the Reference Case 1.
[c] Value based on condenser capacity, and condenser HTF capacitance 0.4379 kW K^{-1} from the Reference Case 1.
[d] Values shown for R-134a. Values for other refrigerants vary by ±0.02 K.

Table 12. Inputs for simulations with optimized tube circuitry at the high-capacity range.

Parameter	Unit	Value		
Cooling capacity	kW	3.05	3.55	4.05
Comp. isen. eff. (η_s)	--	0.81	0.83	0.77
Comp. vol. eff. (η_v)	--	0.78	0.82	0.75
LLSL-HX effectiveness [a]	--	0 (0.4)	0 (0.4)	0 (0.4)
HTF ΔT: evap.[b]	K	8.60	10.00	11.41
HTF ΔT: cond.[c,d]	K	3.32	3.94	4.70
HTF inlet T: evap.	°C	28.01	28.01	28.01
HTF inlet T: cond.	°C	32.69	32.69	32.69
Number of tubes: evap.	--	14	14	14
Number of tubes: cond.	--	20	20	20
Superheat: evap. out	K	15	15	15
Subcooling: cond. out	K	5	5	5
$\Delta T_{dew,suc}$: suction line	°C	0.52	0.90	1.83
$\Delta T_{dew,dis}$: discharge line	°C	0.62	0.73	0.83

[a] Value for simulations with the: basic cycle (LLSL-HX cycle).
[b] Value based on cooling capacity, and evaporator HTF capacitance 0.3548 kW K^{-1} from Reference Case 3.
[c] Value based on condenser capacity, and condenser HTF capacitance 1.0822 kW K^{-1} from Reference Case 3.
[d] Values shown for R-410A. Values for other refrigerants vary by ±0.07 K.

4.2 Simulation results

Configuration 1: Equal compressor efficiency, basic cycle

Fig. 15 (left) shows the simulated COPs for all refrigerants with equal compressor efficiency, at the conditions from the medium-pressure refrigerants (Section 2.2.1). The COPs are shown normalized by the regression of R-134a experimental basic-cycle COPs from Fig. 3. The spread in COP amongst the medium-pressure refrigerants (i.e., difference in highest COP, R-134a, and lowest COP, R-515B) was only (3 to 9) %, compared with (12 to 33) % for the experimental tests (Fig. 4) where compressor efficiencies weren't equal (Fig. 8). Therefore, differences in compressor efficiency with different refrigerants accounted for a large portion of the spread in the experimentally measured COPs.

Fig. 15 (left) shows the high-pressure refrigerants (R-410A, R-32, R-454B, R-452B) had lower COP than the medium-pressure refrigerants (R-134a, R-513A, Tern-1, R-450A, R-515B, R-1234yf) at low capacity (1.3 kW), but higher COP at high capacity (1.7 kW) where the ΔP penalty was lower for high-pressure refrigerants [14].

Configuration 2: Equal compressor efficiency, basic cycle, optimized tube circuitry

With optimized evaporator and condenser tube circuitry, the spread in COP amongst the medium-pressure refrigerants reduced to about 3 %, compared to (3 to 9) % without circuit optimization (i.e., *Configuration 1*). The circuit optimization was particularly beneficial at high capacity for the lowest-pressure, lowest-density refrigerants (R-515B and R-1234yf) whose non-optimized HXs had high velocity and ΔP (particularly in the evaporator).

The high-pressure refrigerants always outperformed the medium-pressure refrigerants, by about (1 to 6) % (Fig. 15, center). The best high-pressure refrigerant, R-32, had COP about 3 % higher than the best medium-pressure refrigerant, R-134a.

Configuration 3: Equal compressor efficiency, LLSL-HX cycle, optimized tube circuitry

The LLSL-HX increased medium-pressure refrigerants' COP (1.0 to 1.5) % and decreased the high-pressure refrigerants COP (0 to 1) % (Fig. 15, right). This is consistent with the observation from [6] that the LLSL-HX benefits refrigerants with higher molar heat capacity, but doesn't benefit, and may penalize, refrigerants with low molar heat capacity (Table 3). The rankings of the refrigerants didn't change with the addition of the LLSL-HX. The superheat, 15 K, was relatively large for use with a LLSL-HX but was selected for clearer comparison with results from the basic cycle. By reducing the superheat to 5 K, the COP benefit of the LLSL-HX (not shown) increased about 0.5 % (percentage points).

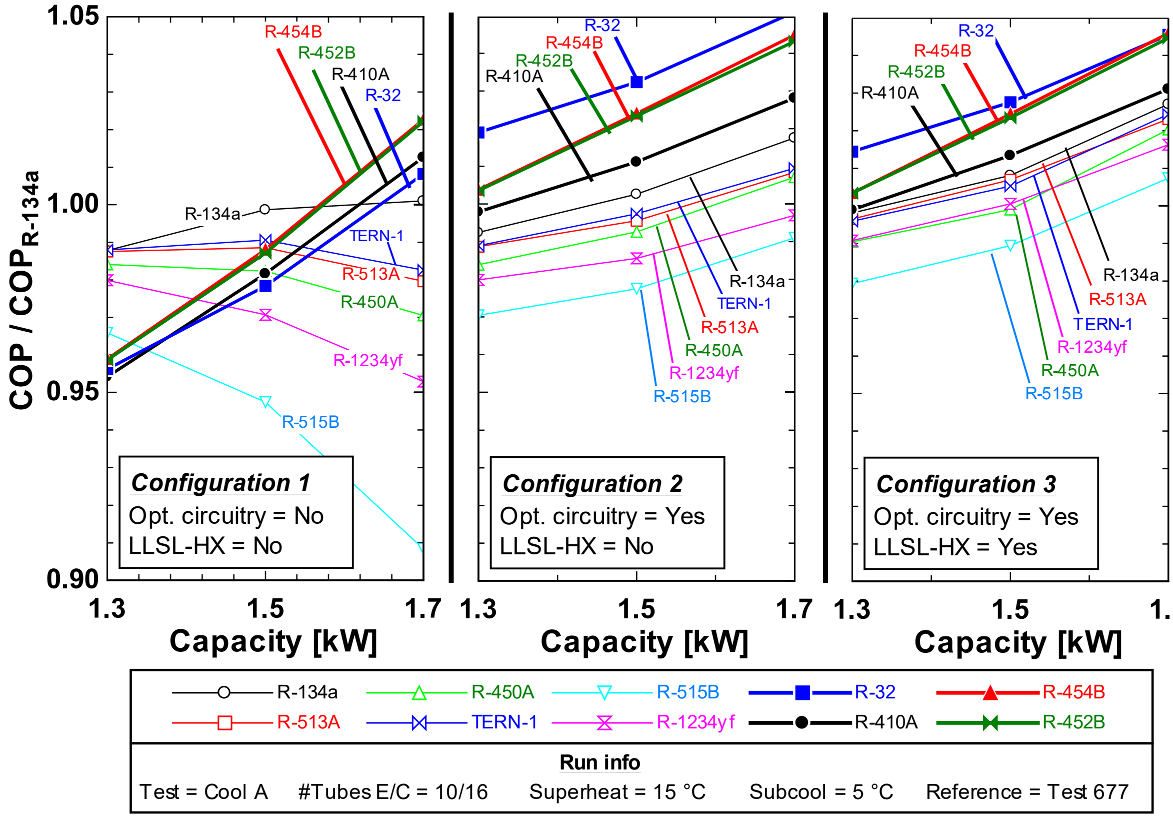

Fig. 15. Simulated normalized COP for the: (left) basic cycle without circuit optimization, (center) basic cycle with circuit optimization, and (right) LLSL-HX cycle with circuit optimization. Values normalized by regression of R-134a experimental basic-cycle COPs.

The optimal number of evaporator and condenser circuits ($NC_{opt,evap}$, $NC_{opt,cond}$) ranged (0.5 to 1.5) to achieve maximum COPs for the basic cycle (Fig. 16). The test apparatus was configured for optimal performance with R-134a at 1.5 kW, so NC_{opt} was near 1 for that condition. For the medium-pressure refrigerants, $NC_{opt,evap} \approx 1$ at 1.3 kW capacity, and increased to (1.35 to 1.55) circuits at 1.7 kW capacity. The additional circuits reduced the mass flux and ΔP at the high capacity. For the high-pressure refrigerants, $NC_{opt,evap}$ was lower, (0.5 to 0.9), since the mass flux could be increased to enlarge the HTC without significant ΔP penalty. The $NC_{opt,evap}$ increased with capacity, but not as much as for the medium-pressure refrigerants. For the condenser, $NC_{opt,cond}$ for the medium-pressure refrigerants ranged (0.9 to 1.1) and varied little with capacity. The $NC_{opt,cond}$ was lower for the high-pressure refrigerants (0.6 to 0.7) than for the medium-pressure refrigerants, for the same reasons as in the evaporator. Interestingly, $NC_{opt,cond}$ decreased as the capacity increased, indicating greater marginal benefit of enhanced HTC than marginal penalty of additional ΔP_{cond}. The optimal mass flux for medium-pressure refrigerants ranged: (140 to 170) $kg\,s^{-1}\,m^{-2}$ in the evaporator and (140 to 230) $kg\,s^{-1}\,m^{-2}$ in the condenser. For the high-pressure refrigerants, the optimal mass flux ranged: (160 to 180) $kg\,s^{-1}\,m^{-2}$ in the evaporator and (140 to 270) $kg\,s^{-1}\,m^{-2}$ in the condenser.

Note that CYCLE_D-HX selected non-integer NC_{opt} (e.g., 0.7, 1.3, in Fig. 16), because this system is small, and the heat exchangers only have a single circuit. The results can be scaled to a larger system to yield a practicable integer number of circuits. For example, at 1.5 kW capacity R-515B had $NC_{opt,evap} \approx 1.3$ and $NC_{opt,cond} \approx 1.1$. For a system with 10x capacity of 15 kW and 10x number of total tubes, $NC_{opt,evap} \approx 13$ and $NC_{opt,cond} \approx 11$.

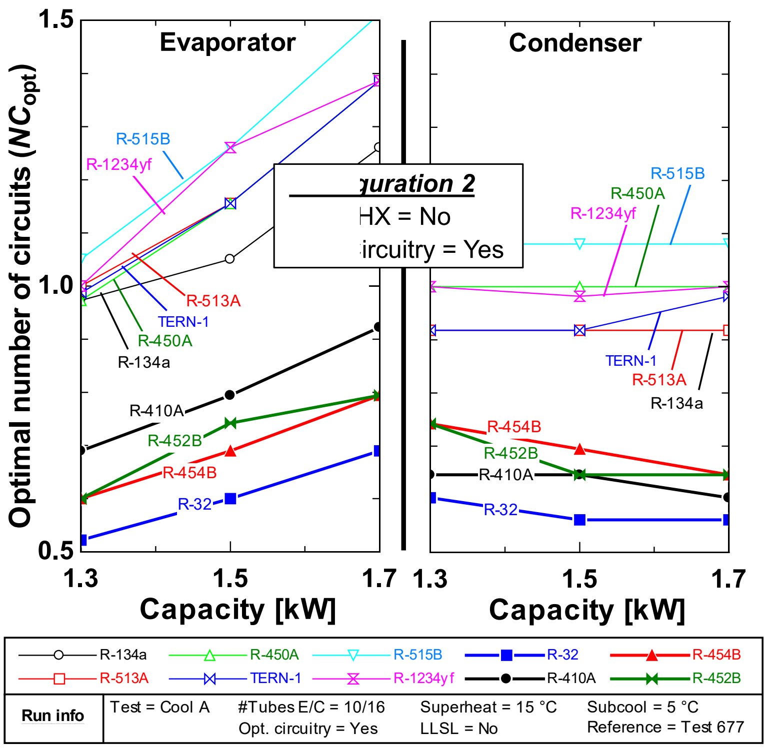

Fig. 16. Optimal number of tube circuits selected by the model for the basic cycle: (left) evaporator, (right) condenser.

The results (not shown) for the higher-capacity simulations (Table 12) were very similar to the lower-capacity simulations in terms of relative refrigerant ranking, effect of optimizing tube circuitry, and effect of adding the LLSL-HX to the basic cycle.

Finally, Fig. 17 shows the COPs with optimized tube circuitry (i.e., Fig. 15) vs. GWP, for capacity 1.5 kW. For the medium-pressure refrigerants in the basic cycle, compared to R-134a with GWP = 1300 and safety group 'A1' (Table 3), the other refrigerants were (GWP, $COP/COP_{R\text{-}134}$, safety group): Tern-1 (640, -0.2 %, A1), R-513A (573, -0.4 %, A1), R-450A (547, -0.7 %, A1), R-515B (299, -2.3%, A1), R-1234yf (<1, -1.4%, A2L). The results with the LLSL-HX were similar, with R-513A and Tern-1 achieving COP within 0.3 % of R-134a. Generally, as the refrigerants' GWP reduced so did the COP. R-1234yf had the lowest GWP and better COP than R-515B (and R-450A with the LLSL-HX), but has a '2L' flammability rating. Thus, there are lower-GWP, non-flammable options for R-134a with small COP penalty.

For the high-pressure refrigerants in the basic cycle, compared to R-410A with GWP = 1924, $COP/COP_{R\text{-}134}$ = +1.0 %, and safety group 'A1', the other refrigerants were: R-32 (677, +3.2 %, A2L), R-454B (467, +2.4 %, A2L), R-452B (676,+2.3 %, A2L). The results with the LLSL-HX were similar. The lower-GWP fluids provide benefit with higher COP than R-410A but have the '2L' flammability rating. R-32 and R-454B were the best lower-GWP options.

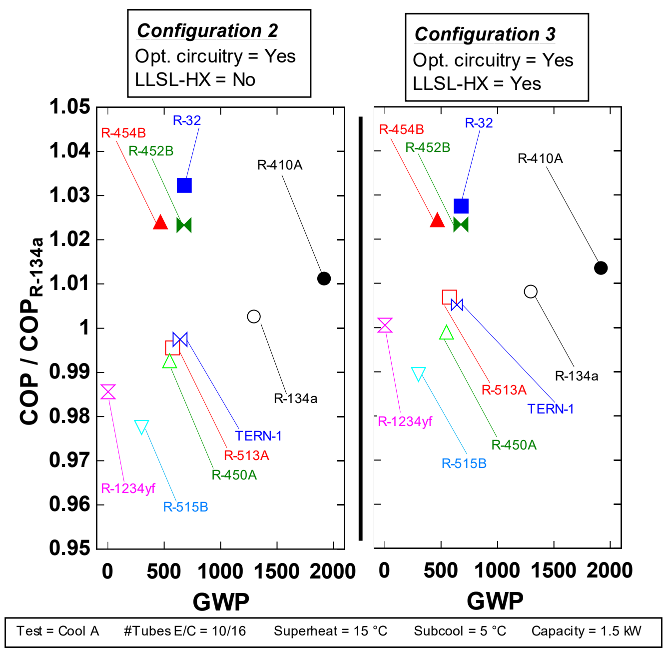

Fig. 17. Simulated normalized COP vs GWP for the: (left) basic cycle with circuit optimization, (right) LLSL-HX cycle with circuit optimization.

5 Conclusions

CYCLE_D-HX is a semi-theoretical model that simulates performance of a vapor-compression cycle for specified temperature profiles of the heat source and heat sink. The evaporator and condenser refrigerant saturation conditions can optionally be predicted based on physical models of the two-phase HTC and ΔP. Further, CYCLE_D-HX can optimize the circuiting of a fixed set of evaporator and condenser tubes. The model is useful for preliminary refrigerant screening and system design for vapor-compression cycles using tube-based forced-convection HXs.

The focus of this study was to experimentally validate the model, and to demonstrate the model's ability to evaluate refrigerants' maximum performance potential. A small heat pump apparatus with an optional LLSL-HX was used to test medium-pressure refrigerants: R-134a, and five lower-GWP replacements including: R-513A, R-450A, Tern-1 (R-134a/1234yf/1234ze(E) 49.2/33.8/17.0 % by mass), R-515B, and R-1234yf. High-pressure refrigerants were also tested, including R-410A, and three lower-GWP replacements: R-32, R-454B, and R-452B. The model was tuned with a limited set of 'Reference Case' experimental data, and used to predict system performance for all tested refrigerants over a range of capacity. Lastly, simulations were used to compare the refrigerants' maximum performance potential by applying equal compressor efficiency, optimized HX tube circuitry, and the LLSL-HX. The key findings include:

Experimental validation (Section 3.2)

- The model overpredicted COP and Q_{vol} by (0 to 3) %, for the basic cycle.
- The model generally predicted the ΔP within ±10 %, though it was off by as much as 20 % for R-1234yf.
- The discrepancy between the model and the experimental results was largely attributed to overprediction of HTC in the evaporator and/or condenser for hydrofluoroolefins (HFOs, i.e., R-1234yf) and HFO blends (i.e., R-513A, Tern-1, R-450A, R-515B, R-454B, R-452B). CYCLE_D-HX calculates the HTC using the flow-pattern map method of [29], [30] developed using HFC refrigerants, which may be overpredicting the HTC for HFOs and HFO blends.
- The model generally predicted the COP ranking from the experimental tests, which supports previous studies that used CYCLE_D-HX to screen and rank lower-GWP replacement refrigerants [19]–[22].

Simulated refrigerant maximum performance potential (Section 4.2)

- The model enabled comparison of medium- and high-pressure refrigerants at the same capacity, HX size, and compressor efficiency, which couldn't be done experimentally due to hardware limitations.
- Proper design can significantly reduce the spread in COP amongst refrigerants (i.e., difference between highest and lowest COP). In the experimental tests with medium-pressure refrigerants the COP spread was (12 to 33) %. In the simulations with equal compressor efficiency (*Configuration 1*) the spread reduced to (3 to 9) %. Simulations with optimized HX tube circuitry (*Configuration 2*) showed even less spread, about 3 %.

The optimization was most beneficial to the lowest-pressure, lowest-Q_{vol} refrigerants R-515B and R-1234yf.

- With optimized HX tube circuitry, adding the LLSL-HX (*Configuration 3*) increased the COP by (1.0 to 1.5) % compared to *Configuration 2* for refrigerants with higher molar-heat-capacity (here, the medium-pressure refrigerants), and decreased the COP by (0 to 1.0) % for the refrigerants with lower molar-heat-capacity (here, the high-pressure refrigerants).
- The medium-pressure, lower-density refrigerants performed best with more evaporator and condenser tube circuits. This reduced refrigerant mass flux, which reduced ΔP.
- The high-pressure, higher-density refrigerants performed best with fewer evaporator and condenser circuits. This increased mass flux and HTC, without significant ΔP penalty.
- The lower-GWP medium-pressure refrigerants had COP (0.2 to 2.3) % less than R-134a.
- The lower-GWP high-pressure refrigerants had COP (2.3 to 3.2) % higher than R-410A.

References

[1] UNEP, “Montreal Protocol on Substances That Deplete the Ozone Layer.” New York, NY, USA, 1987, [Online]. Available: https://www.unep.org/ozonaction/who-we-are/about-montreal-protocol.

[2] M. J. Molina and F. S. Rowland, “Stratospheric sink for chlorofluoromethanes: chlorine atom-catalysed destruction of ozone,” *Nature*, vol. 249, pp. 810–812, 1974, [Online]. Available: https://www.nature.com/articles/249810a0.

[3] M. O. McLinden and R. Radermacher, “Methods for Comparing the Performance of Pure and Mixed Refrigerants in the Vapor Compression Cycle,” *Int. J. Refrig.*, vol. 10, no. 6, pp. 318–325, Nov. 1987, doi: https://doi.org/10.1016/0140-7007(87)90117-4.

[4] P. A. Domanski and M. O. McLinden, “A Simplified Cycle Simulation Model for the Performance Rating of Refrigerants and Refrigerant Mixtures (Paper 132),” in *International Refrigeration and Air Conditioning Conference*, 1990, pp. 466–475, [Online]. Available: http://docs.lib.purdue.edu/iracc/132.

[5] P. A. Domanski and M. O. McLinden, “A simplified cycle simulation model for the performance rating of refrigerants and refrigerant mixtures,” *Int. J. Refrig.*, vol. 15, no. 2, pp. 81–88, Jan. 1992, doi: https://doi.org/10.1016/0140-7007(92)90031-O.

[6] P. A. Domanski, D. A. Didion, and J. P. Doyle, “Evaluation of suction-line/liquid-line heat exchange in the refrigeration cycle,” *Int. J. Refrig.*, vol. 17, no. 7, pp. 487–493, Jan. 1994, doi: https://doi.org/10.1016/0140-7007(94)90010-8.

[7] S. A. Klein, D. T. Reindl, and K. Brownell, “Refrigeration system performance using liquid-suction heat exchangers,” *Int. J. Refrig.*, vol. 23, no. 8, pp. 588–596, Dec. 2000, doi: https://doi.org/10.1016/S0140-7007(00)00008-6.

[8] J. Pannock and D. A. Didion, *The Performance of Chlorine-Free Binary Zeotropic Refrigerant Mixtures in a Heat Pump*. Gaithersburg, MD, USA: National Institute of

Standards and Technology, USA, 1991.

[9] P. A. Domanski, D. A. Didion, W. J. Mulroy, and J. Parise, "A Simulation Model and Study of Hydrocarbon Refrigerants for Heat Pump Systems," 1994.

[10] J. S. Brown, S. F. Yana-Motta, and P. A. Domanski, "Comparitive analysis of an automotive air conditioning systems operating with CO2 and R134a," *Int. J. Refrig.*, vol. 25, no. 1, pp. 19–32, Jan. 2002, doi: https://doi.org/10.1016/S0140-7007(01)00011-1.

[11] R. P. McEnaney, Y. C. Park, J. M. Yin, and P. S. Hrnjak, "Performance of the Prototype of a Transcritical R744 Mobile A/C System (Paper 1999-01-0872)," in *SAE International Congress and Exposition*, 1999, pp. 1–10.

[12] R. P. McEnaney, D. E. Boewe, J. M. Yin, Y. C. Park, and C. W. Bullard, "Experimental Comparison of Mobile A/C Systems When Operated with Transcritical CO2 Versus Conventional R134a, Paper #402," 1998, [Online]. Available: http://docs.lib.purdue.edu/iracc/402.

[13] J. S. Brown, Y. Kim, and P. A. Domanski, "Evaluation of carbon dioxide as R-22 substitute for residential air-conditioning," *ASHRAE Trans.*, vol. 108 PART 2, pp. 954–963, 2002.

[14] R. Brignoli, J. S. Brown, H. M. Skye, and P. A. Domanski, "Refrigerant performance evaluation including effects of transport properties and optimized heat exchangers," *Int. J. Refrig.*, vol. 80, Aug. 2017, doi: https://doi.org/10.1016/j.ijrefrig.2017.05.014.

[15] J. S. Brown, R. Brignoli, and P. A. Domanski, "CYCLE_D-HX: NIST vapor compression cycle model accounting for refrigerant thermodynamic and transport properties, version 1.0, user's guide," Gaithersburg, MD, Dec. 2017. doi: https://doi.org/10.6028/NIST.TN.1974.

[16] J. S. Brown, R. Brignoli, and P. A. Domanski, "CYCLE_D-HX: NIST Vapor Compression Cycle Model Accounting for Refrigerant Thermodynamic and Transport Properties." 2021, Accessed: Mar. 26, 2021. [Online]. Available: https://www.nist.gov/services-resources/software/cycled-hx-nist-vapor-compression-cycle-model-accounting-refrigerant.

[17] UNEP, *Amendment to the Montreal Protocol on Substances that Deplete the Ozone Layer, Kigali, Rwanda, 15 October 2016, C.N.872.2016.TREATIES-XXVII.2.f.* 2016.

[18] EU, *Regulation (EU) No 517/2014 of the European Parliament and of the Council of 16 April 2014 on fluorinated greenhouse gases and repealing Regulation (EC) No 842/2006*. 2014.

[19] P. A. Domanski, R. Brignoli, J. S. Brown, A. F. Kazakov, and M. O. McLinden, "Low-GWP refrigerants for medium and high-pressure applications," *Int. J. Refrig.*, vol. 84, pp. 198–209, Dec. 2017, doi: https://doi.org/10.1016/J.IJREFRIG.2017.08.019.

[20] I. H. Bell, P. A. Domanski, M. O. McLinden, and G. T. Linteris, "The hunt for nonflammable refrigerant blends to replace R-134a," *Int. J. Refrig.*, vol. 104, pp. 484–495, Aug. 2019, doi: https://doi.org/10.1016/J.IJREFRIG.2019.05.035.

[21] P. A. Domanski, M. O. McLinden, I. H. Bell, and G. T. Linteris, "Low-GWP Alternative Refrigerant Blends for HFC-134a (NIST Technical Note 2014)," Gaithersburg, MD, USA,

2018. doi: https://doi.org/10.6028/NIST.TN.2014.

[22] P. A. Domanski *et al.*, "Low-GWP Alternative Refrigerant Blends for HFC-134a: Interim Report (NISTIR 8395)," 2021. [Online]. Available: https://doi.org/10.6028/NIST.IR.8395.

[23] H. M. Skye, "Data for NIST Technical Note: Validation and Demonstration of a Vapor Compression Cycle Model Accounting for Refrigerant Thermodynamic and Transport Properties." National Institute of Standards and Technology, USA, Gaithersburg, MD, USA, 2022, doi: https://doi.org/10.18434/mds2-2613.

[24] E. W. Lemmon, I. H. Bell, M. L. Huber, and M. O. McLinden, "NIST Standard Reference Database 23: Reference Fluid Thermodynamic and Transport Properties-REFPROP, Version 10.0." National Institute of Standards and Technology, USA, 2018, [Online]. Available: https://www.nist.gov/srd/refprop.

[25] H. M. Skye, "Heat Pump Test Apparatus for the Evaluation of Low Global Warming Potential Refrigerants (NIST NT 1895)," Gaithersburg, MD, USA, 2015. doi: https://doi.org/10.6028/NIST.TN.1895.

[26] ANSI/ASHRAE, "ANSI/ASHRAE Standard 34-2019: Designation and Safety Classification of Refrigerants." Amer. Soc. Heating, Ref. Air-Conditioning Eng. Inc., Atlanta, GA, 2019, [Online]. Available: https://www.ashrae.org/technical-resources/standards-and-guidelines/ashrae-refrigerant-designations.

[27] IPCC, "Climate Change 2013: The Physical Science Basis. Contribution of Working Group I to the Fifth Assessment Report of the Intergovernmental Panel on Climate Change," [Myhre, G.; Shindell, D.; Bréon, F.-M.; Collins, W.; Fuglestvedt, J.; Huang, J.; Koch, D.; Lamarque, J.-F.; Lee, D.; Mendoza, B.; Nakajima, T.; Robock, A.; Stephens, G.; Takemura, T.; Zhang, H]. Cambridge University Press, Cambridge, United Kingdom and New York, NY, USA, 2013. doi: https://doi.org/10.1017/CBO9781107415324.018.

[28] AHRI, *AHRI Standard 210/240: Performance Rating of Unitary Air-Conditioning & Air-Source Heat Pump Equipment*. Arlington, VA: Air-conditioning, Heating, & Refrigeration Institute, 2017.

[29] L. Wojtan, T. Ursenbacher, and J. R. Thome, "Investigation of flow boiling in horizontal tubes: Part I—A new diabatic two-phase flow pattern map," *Int. J. Heat Mass Transf.*, vol. 48, no. 14, pp. 2955–2969, Jul. 2005, doi: https://doi.org/10.1016/J.IJHEATMASSTRANSFER.2004.12.012.

[30] L. Wojtan, T. Ursenbacher, and J. R. Thome, "Investigation of flow boiling in horizontal tubes: Part II—Development of a new heat transfer model for stratified-wavy, dryout and mist flow regimes," *Int. J. Heat Mass Transf.*, vol. 48, no. 14, pp. 2970–2985, Jul. 2005, doi: https://doi.org/10.1016/J.IJHEATMASSTRANSFER.2004.12.013.

[31] L. M. Schlager, M. B. Pate, and A. E. Bergles, "Heat transfer and pressure drop during evaporation and condensation of R22 in horizontal micro-fin tubes," *Int. J. Refrig.*, vol. 12, no. 1, pp. 6–14, Jan. 1989.

[32] H. Mueller-Steinhagen and K. Heck, "Simple Friction Pressure Drop Correlation for Two-phase Flow in Pipes.," *Chem. Eng. Process.*, vol. 20, no. 6, pp. 297–308, Dec. 1986, doi: https://doi.org/10.1016/0255-2701(86)80008-3.

[33] J. Y. Choi, M. A. Kedzierski, and P. A. Domanski, "Generalized Pressure Drop Correlation for Evaporation and Condensation in Smooth and Micro-fin Tube," 2001, [Online]. Available: https://tsapps.nist.gov/publication/get_pdf.cfm?pub_id=860849.

Appendix A. List of Symbols, Abbreviations, and Acronyms

ANSI	American National Standards Institute
ASHRAE	American Soc. of Heating, Refrigerating and Air-Conditioning Engineers.
CI	confidence interval (95 % used here, with coverage factor, k, of 2)
COP	coefficient of performance
CYCLE-11	Model for vapor compression cycle with a LLSL-HX
CYCLE-11.UA	Same as CYCLE-11, but optionally includes refrigerant HTC and ΔP_r
CYCLE-11.UA-CO_2	Same as CYCLE-11.UA, but for transcritical CO_2 cycles
CYCLE_D-HX	NIST vapor compression cycle model accounting for refrigerant thermodynamic and transport properties
EEV	electronic expansion valve
GWP	global warming potential
HFC	hydrofluorocarbon
HFO	hydrofluoroolefin
HTC	heat-transfer coefficient
HTF	heat-transfer fluid
HVAC&R	heating, ventilating, air-conditioning, and refrigeration
HX	heat exchanger
ID	inner diameter
LLSL-HX	liquid-line/suction-line heat exchanger
NIST	National Institute of Standards and Technology, United States
OD	outer diameter
R-114	1,2-Dichlorotetrafluoroethane
R-125	Pentafluoroethane
R-134a	1,1,1,2-Tetrafluoroethane
R-22	Chlorodifluoromethane
R-227ea	1,1,1,2,3,3,3-Heptafluoropropane
R-32	Difluoromethane
R-410A	refrigerant blend of R-32/125 with 50/50 % by mass
R-450A	refrigerant blend of R-134a/1234ze(E) with 42.0/58.0 % by mass
R-452B	refrigerant blend of R-32/125/1234yf with 67.0/7.0/26.0 % by mass
R-454B	refrigerant blend of R-32/1234yf with 68.9/31.1% by mass
R-513A	refrigerant blend of R-134a/1234yf with 44.0/56.0 % by mass
R-515B	refrigerant blend of R-227ea/1234ze(E) with 8.9/91.1 % by mass
R-1234yf	2,3,3,3-Tetrafluoropropene
R-1234ze(E)	trans-1,3,3,3-Tetrafluoropropene
REFPROP	NIST Reference Fluid Thermodynamic and Transport Properties Database
Tern-1	Blend of R-134a/1234yf/1234ze(E) (49.2/33.8/17.0 mass fraction, %)
Tol	tolerance

Symbols

A	area (m^2)
c	specific heat ($kJ\,kg^{-1}\,K^{-1}$)
$factor_{\Delta p}$	refrigerant pressure-drop multiplication factor
h	heat-transfer coefficient ($kW\,m^{-2}\,K^{-1}$)
i	specific enthalpy ($kJ\,kg^{-1}$)
k	uncertainty coverage factor ($k=2$ standard deviations for 95 % confidence interval)
m	mass flow ($kg\,s^{-1}$)
N	compressor speed (Hz)
NC	number of refrigerant tube circuits in heat exchanger
NBP	normal boiling point, at 101.325 kPa (°C)
P	pressure (kPa)
Q	heat transfer (W, kW)
Q_{vol}	volumetric capacity, $Q_{vol} = Q_{evap}\, m_r^{-1}\, v_1^{-1}$ ($kJ\,m^{-3}$)
R	thermal resistance ($K\,kW^{-1}$)
T	temperature (°C), temperature difference (K)
ΔT_{hx}	harmonic-mean effective temperature difference between refrigerant and HTF (K)
ΔT_{dew}	dewpoint temperature change = $T_{dew,in} - T_{dew,out} = T(P_{in}, x=1) - T(P_{out}, x=1)$
To	torque (N m)
s	specific entropy ($kJ\,kg^{-1}\,K^{-1}$)
U	overall heat transfer coefficient ($kW\,m^{-2}\,K^{-1}$)
UA	overall heat exchanger conductance ($kW\,K^{-1}$)
v	specific volume ($m^3\,kg^{-1}$)
x	thermodynamic vapor quality

Greek symbols

Δ	difference, change
η	compressor efficiency

Subscripts

avg	average
cond	condenser
cr	critical
dis	discharge line
dew	dewpoint (i.e., where x=1)
evap	evaporator
hx	heat exchanger
HTF	heat transfer fluid
opt	optimized
p	constant pressure (specific heat)
r	refrigerant
s	isentropic efficiency
sat	average saturation temperature
suc	suction line (compressor)
v	volumetric efficiency
1-13	thermodynamic state defined in Fig. 2 (1 = compressor suction)

Appendix B. Test Apparatus Detail

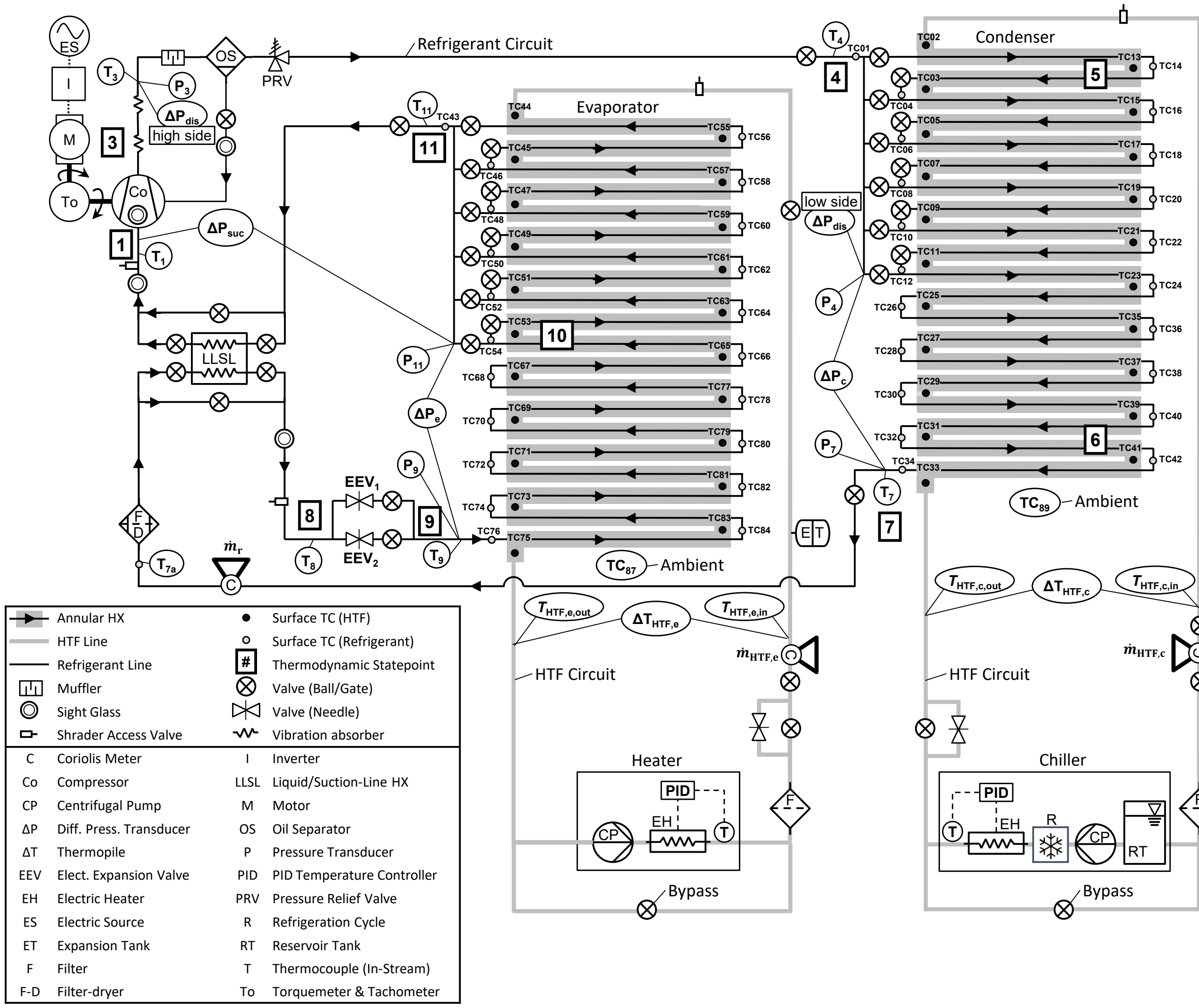

Fig. 18. Detailed test apparatus schematic.

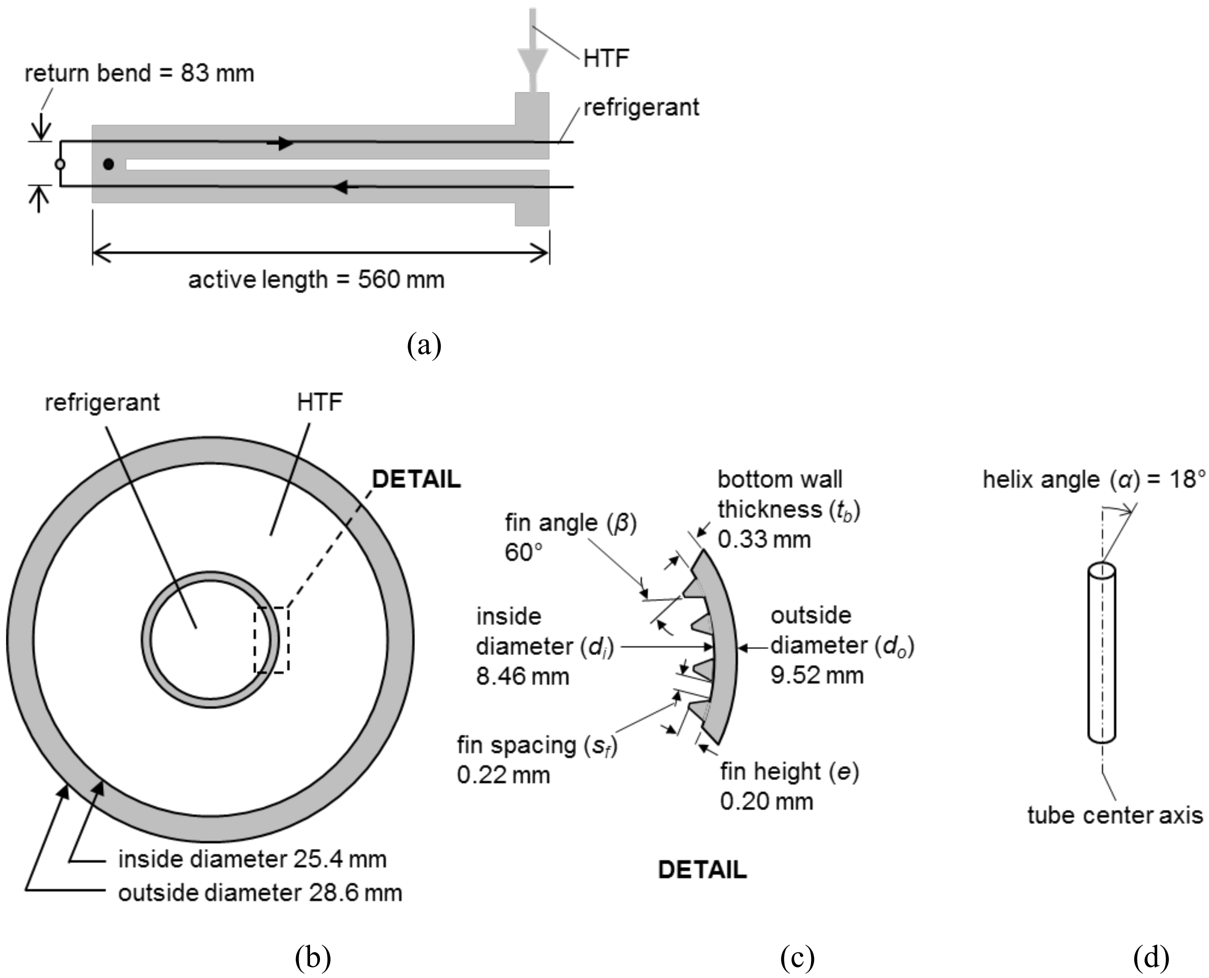

Fig. 19. Schematics of annular heat exchanger including (a) refrigerant tube lengths, (b) cross section of annular heat exchanger, (c) detailed cross-section of microfin tube, and (d) helix angle of microfins.